3D analysis of railway induced vibrations on skew girder bridges including ballast track-bridge interaction effects

J.C. Sánchez-Quesada[a,*], A. Romero[b], P. Galvín[b,c], E. Moliner[a], M.D. Martínez-Rodrigo[a]

[a] *Universitat Jaume I, Department of Mechanical Engineering and Construction, Avda. Sos Baynat s/n, ES-12071 Castellón, Spain*

[b] *Escuela Técnica Superior de Ingeniería, Universidad de Sevilla, Camino de los Descubrimientos s/n, ES-41092 Sevilla, Spain*

[c] *ENGREEN, Laboratory of Engineering for Energy and Environmental Sustainability, Universidad de Sevilla, Camino de los Descubrimientos s/n, ES-41092 Sevilla, Spain*

Abstract

This work is devoted to the analysis of the vibratory response of High-Speed (HS) multi-track railway bridges composed by simply-supported spans. In particular, it aims to investigate the influence of three geometrical aspects usually disregarded in numerical models used to evaluate the Serviceability Limit State of traffic safety in such structures: (i) the deck obliquity, (ii) the presence and correct execution of transverse diaphragms at the supports, and (iii) the number of successive simply-supported spans weakly coupled through the ballast track layer. The influence of these aspects is analysed from the correlation of a detailed numerical model and experimental measurements on an in-service High Speed (HS) multi-track railway bridge. From the reference model, a set of variants accounting for different levels of deck obliquity and diaphragm configurations are envisaged and the maximum transverse acceleration over the platform is determined under railway excitation. The analysis is extended to bridges with an increasing number of successive spans. Special attention is paid to the particular location of the maximum response and to the participation of modes different from the longitudinal bending one. Finally, a numerical–experimental comparison of the bridge response under two train passages is presented for the straight and oblique models, and the response adjustment along with the actual bridge performance are assessed.

Keywords: Railway bridges, vertical acceleration, skewness, transverse diaphragms, ballast track, experimental measurements, resonance.

1. Introduction

Sustainable transport is a major challenge for improving economic competitiveness and achieving a balanced and climate-neutral development. Raising the share of rail transport is a key objective to decarbonise

*Corresponding author.
Email address: jquesada@uji.es (J.C. Sánchez-Quesada)

the economy [1] and one of the main targets of European research programs. The increase in railway capacity and the aging of the infrastructure require the development of advanced preventive maintenance systems to guarantee the required levels of quality, safety and reliability. Bridges and viaducts are specially critical elements due to their continuous exposure to substantial vibratory conditions under the circulation of passenger and freight trains. In this regard, the development of advanced numerical models updated with experimental measurements able to precisely reproduce the dynamic behaviour of the train-track-bridge system, aligned with ongoing trends of *digital twins*, is essential and constitutes the framework for this research.

Railway bridges may experience excessive transverse vibrations with the increasing demands in terms of speed and axle loads. This can lead to deconsolidation of the ballast in the case of ballast tracks or instantaneous loose of wheel-rail contact in the case of slab tracks, rail misalignment, wheel and rail deterioration, structural damage (i.e. concrete cracks, failure of pre-stressing strands, damage in deck supporting elements), poor passenger comfort, etc. This is specially critical in bridges of short to medium spans with simply-supported (SS) decks undergoing resonance, due to their usually associated low mass [2–5]. For this reason, the maximum vertical acceleration at the deck platform is limited by standards [6], and constitutes one of the most demanding Serviceability Limit States in the design of new bridges or in their assessment under higher traffic requirements.

The dynamic response of railway bridges composed of SS spans is generally dominated by the contribution of the first longitudinal bending mode. Many scientific studies and current standard methods rely on this premise [2, 7–9]. However, there are situations where the contribution of other modes such as torsion or transverse bending may contribute significantly. Such is the case of multi-track bridges with oblique or skew decks of comparable widths and span lengths. Oblique or skew bridges are common in mountainous regions where due to topographical features the bridge superstructure cannot be perpendicular to the abutments and piers. Goicolea and collaborators have identified 50 skew underpasses out of 108 slab portal frames in the Madrid-Zaragoza High Speed Line (HSL) in Spain, and 9 skew SS bridges out of 27 in the same line [10]. In these cases, the use of three-dimensional structural models may become necessary and their calibration is very sensitive to boundary conditions.

The most up-to-date and comprehensive numerical models of railway bridges include an explicit and continuous representation of both the structure and the track, including the rails, railpads, sleepers and ballast bed or track slab [11–14]. In particular, the inclusion of the ballast track permits a more accurate representation of the structure response as (i) it simulates the distributive effect of the axle loads; (ii) it facilitates a more realistic representation of the damping mechanisms along the track; (iii) it acts as a filter of high-frequency contributions; (iv) it accounts for the track-deck composite behaviour due to the shear stress transmission between the rails and the deck through the ballast; and (iv) it permits a more accurate modelling of the deck boundary conditions through the simulation of the coupling exerted by the ballast layer between either adjacent decks or consecutive spans structurally independent in principle. These topics

are a matter of recent investigations [12, 15–19].

Using detailed 3D finite element (FE) models, Nouri and Zahed [20] investigated the effect of the skew angle and diaphragm arrangement on the longitudinal bending moment, shear force and corresponding distribution factors in continuous composite highway bridges and compared numerical analyses to AASHTO LRFD specifications [21]. Also, Deng et al. [22] analysed the influence of the curvature and skew angle under design loading conditions of horizontally curved steel-girder road bridges with integral abutments. Additional contributions devoted to the seismic analysis and assessment of skew highway bridges are [23–26].

With the focus on railway bridges, Ryjáček et al. [27] analysed the modal parameters and dynamic response of a single and long span arch bridge with a 43° skew angle. Experimental and numerical results were presented. The authors highlighted the sensitivity of the model to the boundary conditions, and the influence of the skew angle on the hangers vibrations. Nguyen et al. [10] presented a simplified numerical model based on beam theory, including bending and torsion, and on a closed-form modal analysis for fast calculation of the response of skew bridges subjected to moving loads. Warping and distortion effects of the deck cross-section were neglected. The authors concluded that, the skewness played an important role on the dynamic deflections, while the accelerations were much less affected. With the increase of the span length, the skewness effect was reduced in terms of both, changes in natural frequencies and in maximum accelerations. Jahangiri and Zakeri [28] analysed the effect of the deck obliquity using a 3D detailed slab-track-bridge model of a concrete box girder bridge including vehicle-track interaction. The authors indicated that for skew angles less than 15° the natural frequencies were almost unaffected with respect to the straight case. Higher mode-shapes were more sensitive to the obliquity. Also, contrarily to the previous authors, Jahangiri and Zakeri found that the maximum deflection under passing trains tended to reduce with the skew angle, this not being the case for the accelerations, especially for speeds higher than 300 km/h. Martínez-Rodrigo at al. [29] investigated the dynamic properties of orthotropic plates and their response to moving loads, for different skew angles, flexibility of the supports, and longitudinal bending stiffness. It was concluded that maximum resonance and cancellation conditions associated to the first bending and first torsion modes were not so much affected by the plate obliquity. Nevertheless, the first transverse bending mode, was much more affected and incurred errors approached 20% for the highest obliquity levels and most flexible bridges considered. The same authors in [30] analysed the influence of end diaphragms on the modal parameters and on the train induced vibrations in oblique girder bridges using simplified plate-beam models. The authors concluded that the presence of these elements led to an increase in the natural frequencies, especially of the modes with significant deformation of the cross section. Oblique decks of short span lengths (10-12.5 m) were the most affected. They also highlighted a reduction of the deck maximum acceleration under HS traffic with the end diaphragms, especially in the case of skew decks with a small number of longitudinal girders.

Most of the works found in the literature on this topic analyse bridge decks with closed-type cross

sections, where warping and distortion effects are very small. Also, the presence of the ballast track and the coupling exerted between successive spans at the support sections is generally not included and, as stated by different authors, the dynamic response of skew bridges is significantly affected by the boundary conditions. Based on the foregoing, the aim of this work is to investigate the dynamic performance of oblique railway bridges composed by SS spans and girder decks with end diaphragms, taking into account the weak connection between the spans exerted by the ballast layer. The novelties of this contribution when compared to previous ones are various. First, a 3D detailed FE model for the bridge including an accurate representation of the deck girders and diaphragms in highly-skewed configurations is considered, along with a continuous representation of the ballast track, including its possible degradation at the joint between consecutive spans. Second, the influence of prestressed concrete girder decks transverse diaphragms for two realistic practical implementations (connected and disconnected from the slab) on the bridge modal parameters and on the response under railway traffic is analysed. Third, for the particular type of bridges of study (multi-span highly skewed prestressed concrete girder bridges) the circumstances under which the contribution of modes different from the longitudinal bending ones is determinant for the evaluation of the maximum acceleration at the platform and, therefore, these structures cannot be adequately represented by simple longitudinal beam models is fully addressed. Finally, the influence of the weak connection to adjacent spans in multi-span simply-supported bridges due to the track continuity is investigated, and conclusions are extracted regarding the span where the maximum response takes place and the difference in the response amplitude predicted by single span and multi-span models. To this end, a 3D detailed FE model of an existing and representative skew bridge, the bridge over Jabalón River, is implemented and updated with experimental measurements. Based on this, a catalog of bridge models is defined covering (i) several levels of obliqueness, (ii) three transverse diaphragm configurations and (iii) one, two or three SS spans. Within this catalog, the dynamic properties and maximum dynamic response are evaluated. Special attention is given to the influence of the diaphragms at the end sections and to the participation of modes different from the longitudinal bending one. Finally, the vertical response of Jabalón Bridge under two train passages, measured experimentally, is presented and compared to two numerical predictions, accounting and neglecting the deck obliquity. The numerical predictions are discussed along with the structure performance and final design recommendations are provided.

2. Bridge under study

The structure under study which is used as reference case is the Bridge over Jabalón River, from now on Jabalón Bridge. It belongs to the Madrid-Sevilla HS railway line and it is located in the Ciudad Real-Brazatortas section.

The bridge is composed of three identical simply-supported spans of 24.90 m measured between neoprene

Figure 1: Jabalón Bridge: detail of the girder deck and end diaphragms and general view.

bearings centres. It crosses Jabalón River with a skew angle $\beta = 134°$ (see Figure 2(a)). Notice that the skew angle is defined as the angle between the deck longitudinal axis and the support line measured counterclockwise. Each deck consists of a 30 cm thick, 11.6 m wide cast-in-situ concrete slab resting on five 2.05 m high prestressed concrete I girders (see Figure 2)(b). The girders lean on the supports through steel laminated rubber bearings. The same type of elements restrict the transverse movement of the girders. Regarding the substructure, the outermost sections are supported on reinforced concrete abutments while the inner sections of the three bays lean on wall piers. The deck accommodates two ballast tracks with UIC gauge and an equal eccentricity of 2.15 m, two sidewalks and handrails. The continuously welded UIC60 rails are supported on railpads and fixed with clips to monoblock concrete sleepers separated 0.60 m.

On May 2019 an experimental campaign was performed by the authors on this bridge to characterise the surrounding soil dynamic properties and bridge modal parameters. To this end, 15 Endevco model 86 piezoelectric accelerometers with a nominal sensitivity of 10 V/g were installed underneath the girders of the first span, (span closest to Madrid, shaded in Figure 2(a)) measuring in the vertical direction. The sensors layout is included in Figure 3. The acceleration response was filtered applying two third-order Chebyshev filters with high-pass and low-pass frequencies of 1 Hz and 30 Hz, respectively. The sensors response was recorded under operating conditions for several train passages in both directions, and also under ambient vibration. The frequencies and mode shapes of the bridge were identified from ambient vibration by Stochastic Subspace Identification [31]. Modal dampings were obtained from the free vibration response left by each train passage. For additional details on the experimental campaign the reader is referred to Galvín et al. [32].

In Figure 4 the first five experimental natural frequencies (f_i^{exp}), mode shapes and modal damping ratios ($\zeta_{i,FV}^{exp}$) are included. The bridge presents a fundamental frequency of 6.30 Hz, falling within the frequency limits specified in Eurocode 1 (EC1) for the application of simplified dynamic analysis based on impact coefficients. The corresponding modal damping reaches 3.50 %, which is higher than the value prescribed by

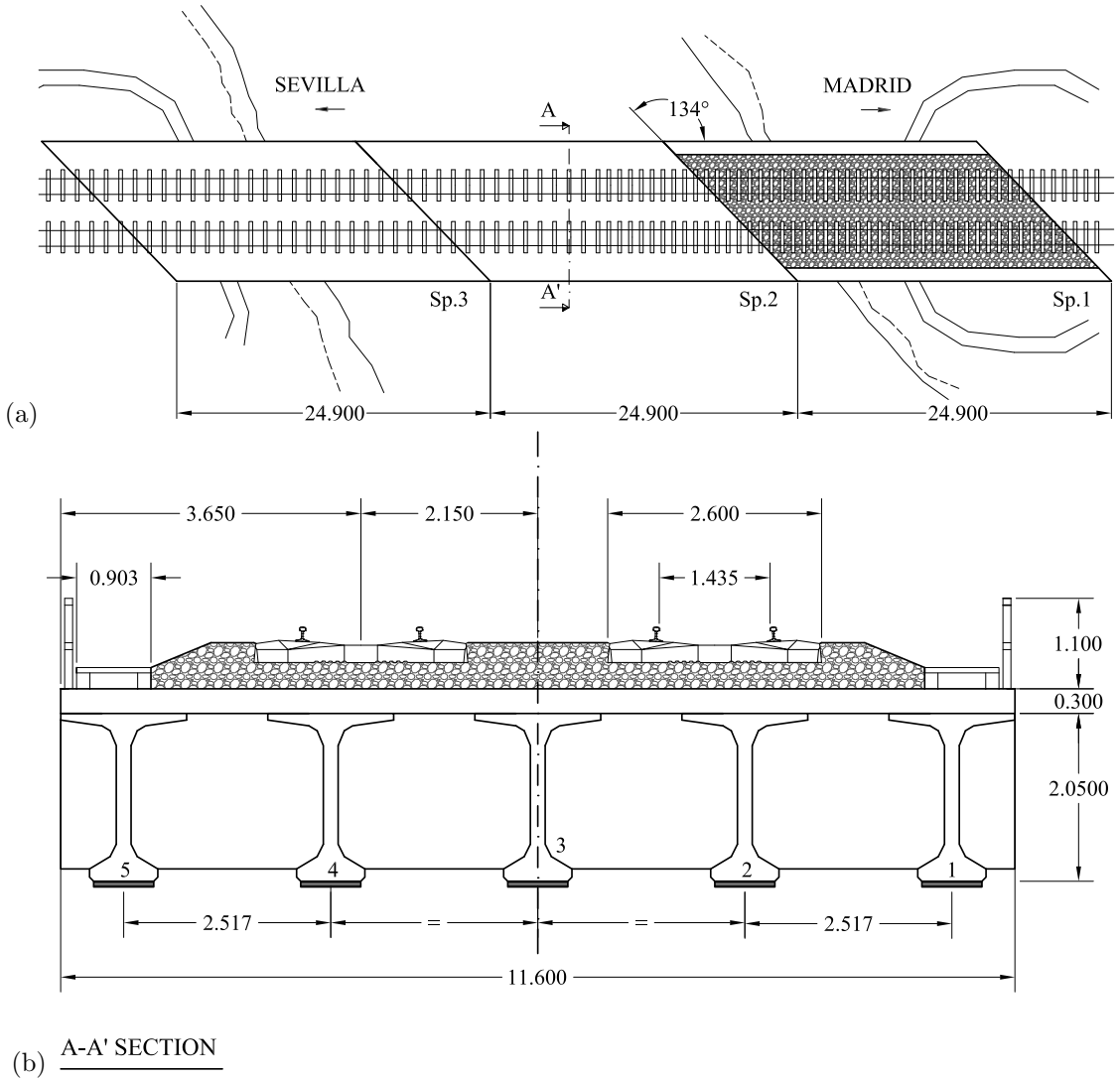

Figure 2: Jabalón Bridge: (a) top view; (b) intermediate cross-section AA'.

standards for the particular bridge type and span length. The first, second and third modes correspond to the first longitudinal bending, first torsion and first transverse bending modes of the instrumented deck. The fourth and fifth modes appear to be a second torsion and second transverse bending modes, respectively.

3. Numerical model

3.1. General description

A 3D continuous FE track-bridge interaction model of Jabalón Bridge is implemented in ANSYS(R)17.1 (see [33]). The model includes the three spans and a track extension of 15 m over the embankment on both sides of the bridge (see Figure 5). This additional track length is equivalent to 25 times the sleeper distance,

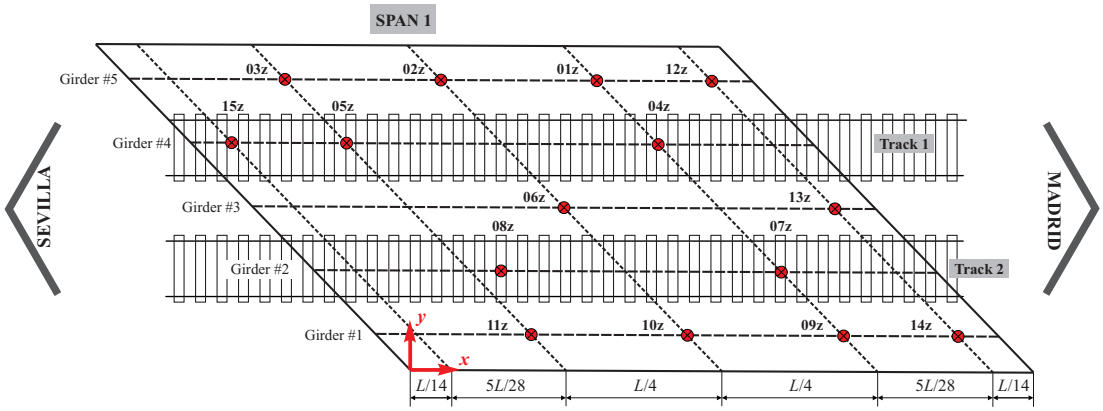

Figure 3: Sensors layout in first span. Units [m].

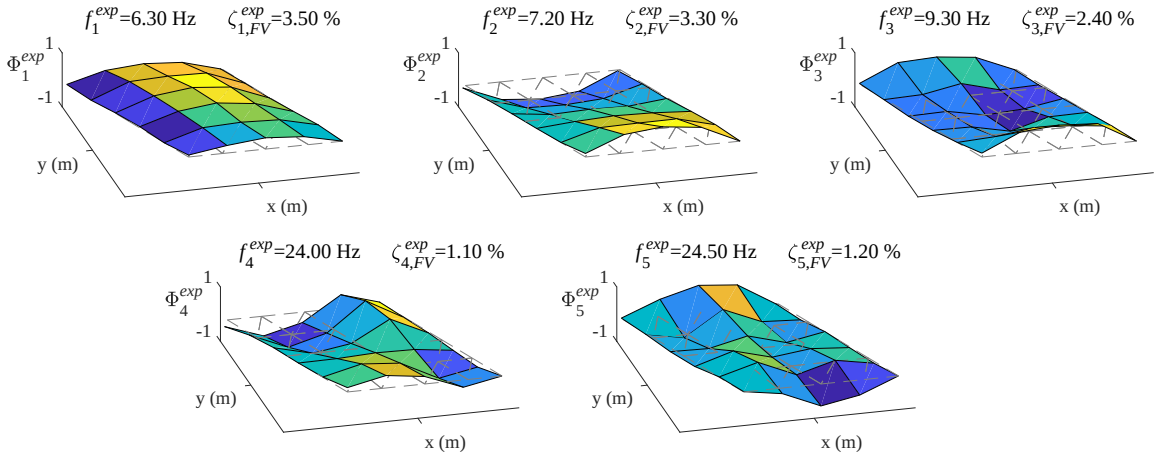

Figure 4: First five natural frequencies, mode shapes and modal damping ratios identified from free vibration (FV) in Jabalón Bridge.

which is considered adequate according to previous works [34, 35] and, also, according to a convergence test performed on the modal parameters. For convenience, the coordinate axes of the model are provided in Figure 5, with axis $z = x \times y$. Henceforth, the longitudinal (parallel to the track), transverse and vertical directions are also referred to as X,Y,Z respectively.

The slabs, longitudinal girders and transverse diaphragms are modelled with shell FEs with 6 degrees of freedom (DOF) per node (SHELL181). The laminated rubber bearings located underneath the girders are meshed with solid elements with 3 DOF per node (SOLID185), considering their real dimensions (width w_{eb}, length l_{eb} and thickness h_{eb}). The bearings acting in the transverse direction are modelled as equivalent linear springs.

In relation to the track, the ballast is divided into (i) a main region meshed with solid elements

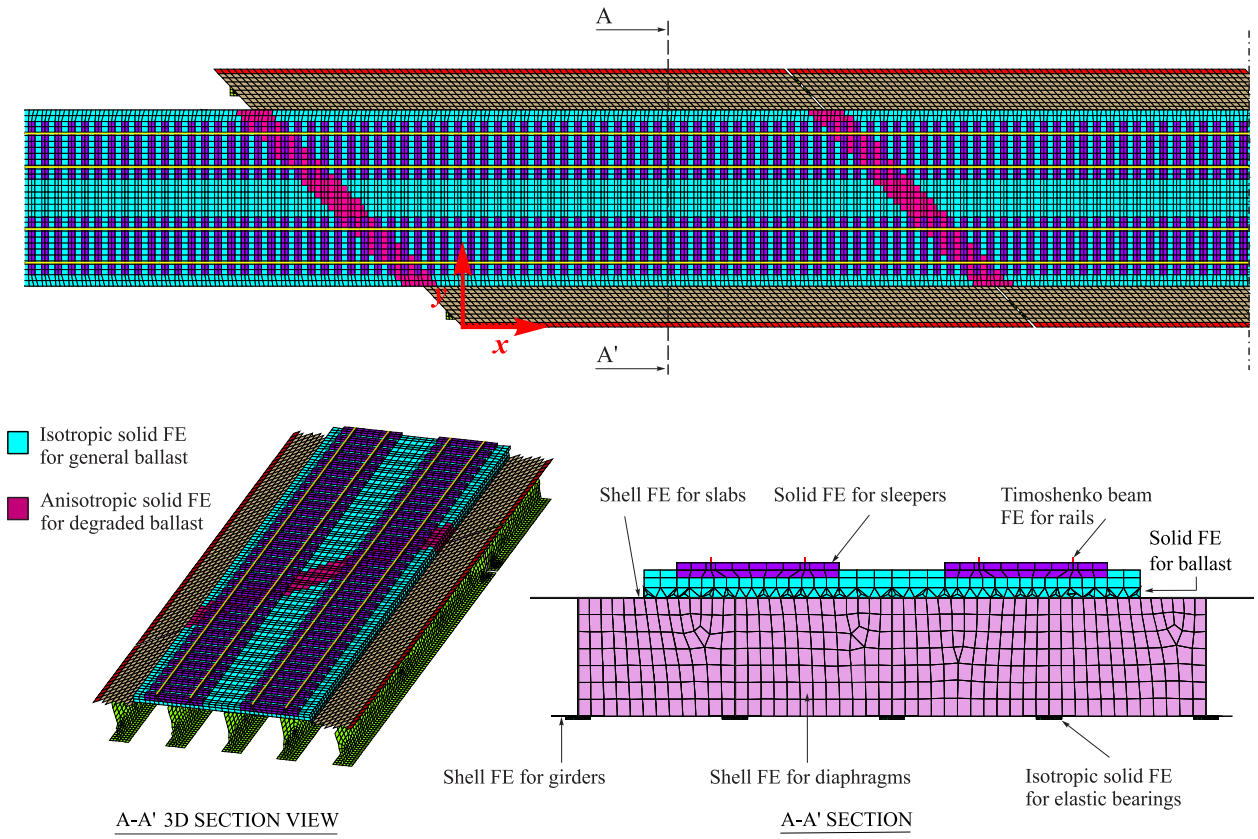

Figure 5: 3D track-bridge FE model of Jabalón Bridge. In the view: plan view of half bridge and track extension, 3D detail of deck section and AA' cross section.

(SOLID185) with isotropic elastic behaviour; and (ii) the volume of ballast in the vicinity of the transverse joints between the spans. In this last case the same solid elements are used but a transversely isotropic material behaviour is assigned. With this approach it is intended to represent different interlocking mechanisms of the ballast granules in the out-of-plane (vertical) and in the in-plane (horizontal) directions, associated to the possible degradation in these regions. The sleepers are meshed into SOLID185 elements with elastic isotropic behaviour. The rails are represented as Timoshenko beam elements with 6 DOF per node (BEAM188). For the rail pads, discrete spring-dashpot elements (COMBIN14) with constant vertical stiffness and viscous damping are adopted. These elements connect the relative vertical displacement between the rails and the sleepers. The vertical force transmitted by the rail pad element is distributed using kinematic constrains over the real contact area between both elements. Finally, in the 15 m of track extension on both sides of the bridge the ballast bed rests on a subgrade layer, which is also meshed with SOLID185 isotropic elastic elements.

Non-structural elements such as the handrails are included in the model as lumped masses (MASS21) uniformly distributed along the two external borders of the deck. Also, the dead weight of the sidewalks is

added to the corresponding areas.

The boundary conditions of the complete model are: (i) the vertical (Z) displacements are restrained at all the nodes at the lower surface of the elastic bearings; (ii) both horizontal (X and Y) displacements of the central node at the lower surface of the bearings along one abutment of each span are also restrained; (iii) at the track extensions, the three translations of all the nodes at the lower plane of the subgrade elements are restrained; and (iv) at both YZ planes that limit the track extensions vertically the three translations of the ballast and subgrade nodes are restrained as well.

The size of the FE mesh is refined so that the wavelengths of the modes up to 30 Hz are adequately reproduced. Also, a mesh convergence study was performed to guarantee an accurate prediction of the natural frequencies and mode shapes of the paired numerical eigenforms as well as of the vertical acceleration levels at the deck under train passage. The final model consists of 854000 elements and 550033 nodes, which correspond to 2251700 DOF.

Concerning the railway excitation a constant moving load model is adopted, neglecting therefore vehicle-structure interaction. This is a deliberate decision since only the evolution of the bridge response under variations of the number of spans, deck obliquity and diaphragm configurations is of interest in this study. Therefore, the effect of geometrical aspects is isolated from other interaction mechanisms that may lead to misleading in the issues investigated. Additionally, as stated by previous research works, vehicle-bridge interaction effects are only relevant at resonance [36]. The bridge vertical response under train passages is numerically obtained by Mode Superposition in the time domain, considering the contribution of modes under 30 Hz. The resulting equations of motion are numerically integrated by the Newmark-β Linear Acceleration algorithm, and the time step is defined as 1/50 times the smallest period of interest.

3.2. Model updating

The numerical model is updated from static and dynamic experimental results as explained in what follows. In Table 1 the model parameters are included. The following nomenclature is used: E, G, ν and ρ stand for elastic and shear modulus, Poisson's ratio, and mass density, respectively. m stands for linear distributed mass. X, Y and Z refer to the longitudinal, transverse and vertical directions previously defined. In the case of the rails, I_{yr} refers to the second moment of area of the cross-section with respect to the principal axis parallel to Y. Concerning the track, K_p and C_p are the vertical stiffness and damping constants of the spring-dashpot elements that represent the rail pads. The sleepers dimensions (length, width and height) and total mass are designated as l_{sl}, w_{sl}, h_{sl} and M_{sl}, respectively, and the distance between consecutive sleepers as d_{sl} . Regarding the ballast, h_b is the height of the ballast layer underneath the sleepers. The total ballast thickness is $h_b + h_{sl}/2$ which is assumed constant and uniform over the platform. A total thickness of 44 cm is considered based on the technical drawings and in situ inspection. This corresponds to a ballast thickness underneath the sleepers of 32 cm, in accordance with current Spanish

regulations [37]. Notice that the main ballast presents isotropic elastic properties E_b and ν_b identical in the three directions, while the degraded ballast elastic constants are expressed as E_{bI}, G_{bIJ} and ν_{bIJ}, where I and J refer to the spatial directions X, Y and Z. The degraded ballast behaviour is defined as transversely isotropic with five independent elastic constants:

$$E_{bX} = E_{bY} \qquad E_{bZ} \qquad G_{bXZ} = G_{bYZ} \qquad \nu_{bXY} \qquad \nu_{bXZ} = \nu_{bYZ} \tag{1}$$

In Equation 1, $E_{bX} = E_{bY}$ are the in-plane elastic moduli, E_{bZ} and $G_{bXZ} = G_{bYZ}$ the out-of-plane elastic and shear moduli, respectively, and ν_{bXY} and $\nu_{bXZ} = \nu_{bYZ}$ the Poisson's ratios. Finally, in Table 1 R_{eb} and R_{ebt} are factors that multiply the vertical and transverse elastic bearings moduli of elasticity in the case of dynamic loads.

The model updating is performed in successive steps. First the elastic modulus of the neoprene bearings at the girder supports, E_{eb}, is calibrated in order to reproduce the experimental static deflection measured during the proof load test performed on the bridge in 1991, before the opening [38]. This first calibration step is performed with the only purpose to set an initial and reasonable value for the elastic modulus of the neoprene bearings under static compressive loads, instead of choosing a value from the literature which may not be realistic for this particular bridge.

Then, the most uncertain parameters are updated based on the modal properties identified from the ambient vibration response during the experimental campaign performed by the authors in 2019 [32]. The correspondence between experimental and numerical modal parameters is quantified through the relative difference between the numerical and experimental frequencies e_{ij} and the Modal Assurance Criterion (MAC_{ij}) [39] of the paired modes as per:

$$e_{ij}\,[100\%] = \frac{f_i^{exp} - f_j^{num}}{f_i^{exp}} \cdot 100 \tag{2}$$

$$\mathrm{MAC}_{ij} = \frac{\left(\Phi_i^{exp,T} \cdot \Phi_j^{num}\right)^2}{\left(\Phi_i^{exp,T} \cdot \Phi_i^{exp}\right) \cdot \left(\Phi_j^{num,T} \cdot \Phi_j^{num}\right)} \tag{3}$$

In the previous equations, superscripts *exp* and *num* denote experimental and numerical, Φ_i^{exp} and Φ_j^{num} are the i-th and j-th experimental and paired numerical mode shape, respectively, f_i^{exp} and f_j^{num} the corresponding natural frequencies and T indicates transpose. Notice that frequency differences and MAC values between unpaired modes are not presented in what follows.

An optimisation iterative procedure implemented in ANSYS(R)17.1 and MATLAB.2018b is carried out based on a Genetic Algorithm (GA) adapted from Haataja's [40], in order to minimise an objective function

involving both the relative difference in natural frequencies and MAC residuals (Equation 4).

$$F_{obj}(P) = \sum_{i=1,j}^{5,j} \left| \frac{e_{ij}\,[100\%]\,(P)}{100} \right| + \sum_{i=1,j}^{5} (1 - \mathrm{MAC}_{ij}(P)) \tag{4a}$$

$$P = (E_b, \rho_b, E_{bX} = E_{bY}, E_g, \rho_g, E_s, \rho_s, R_{eb} = R_{ebt}) \tag{4b}$$

The five modes identified from ambient vibration are included in the updating process (Figure 4). In Equation (4b), P stands for the set of eight model parameters that are subjected to optimisation for this particular bridge model, which are: the ballast density ρ_b, the main and the degraded ballast elastic moduli, E_b and E_{bX}=E_{bY}, the slab and longitudinal girders elastic moduli and density, E_s, E_g, ρ_s and ρ_g and the vertical and transverse neoprene bearings dynamic amplification factor R_{eb}=R_{ebt}. It is known that the choice of a large number of optimisation parameters may lead to an ill-conditioned problem. For this reason, in order to select the proper number of them, a preliminary sensitivity analysis was performed to identify the most influential ones in the modal response of the bridge. A Spearman Correlation Matrix (see Figure 6) was computed including those model parameters which determination entails the most uncertainty. This technique has been also used by previous authors yielding good results [11, 41, 42]. The matrix shows the influence of the model parameters on the frequency differences (referred to unity) and MAC residuals. The Latin Hypercube method is applied with 799 samples.

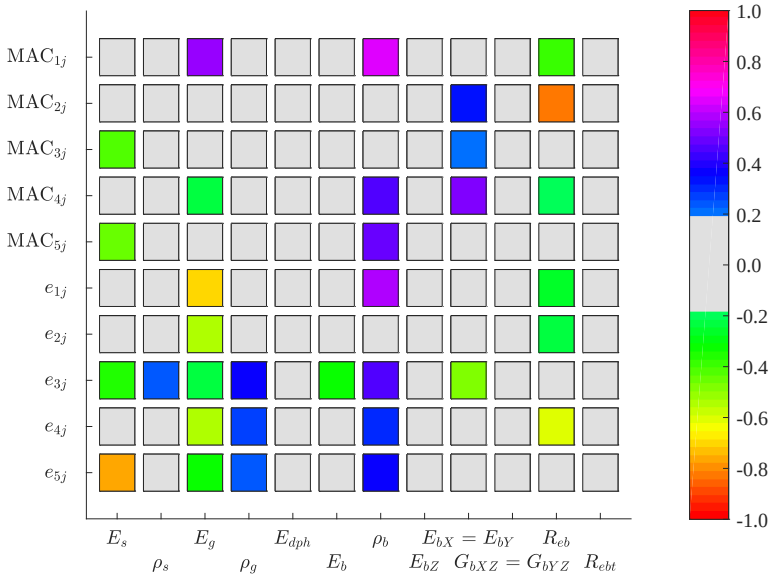

Figure 6: Spearman linear correlation coefficient matrix between frequency difference and MAC of paired modes and model parameters.

In Table 1 initial or nominal values for the model parameters and ranges of variation considered are included based on the bridge technical information available, engineering considerations, the associated

level of uncertainty and the reference values found in the literature and in Standards. The same ranges of variation are used for the sensitivity analysis and in the final updating process. In Figure 6 correlation values between -0.2 and $+0.2$ are excluded from the graphical presentation and considered not-correlated. As can be seen, the eight model parameters included in Equation (4b) exhibit the highest correlation and are selected for the optimisation procedure based on the GA. In this last step, successive model samples are generated from variations of the selected eight parameters within the limits included in Table 1. The final or updated values are also included in the same table. These values are obtained after several runs of the GA to guarantee the stability of the updating procedure, considering a population size of 56 (7 times the number of calibration parameters) and 200 generations. The crossover and mutation probabilities are set to 0.8 and 0.02, respectively, the probability of tournament to 0.7 and the scale of mutation to 0.1. Table 2 shows the results of the model calibration in terms of numerical frequencies (f_j^{num}), frequency differences e_{ij}, and MAC numbers between the experimental i and the paired j numerical mode. In Figure 7 the first five numerical mode shapes and natural frequencies of the updated model are represented. The first longitudinal bending, first torsion and first transverse bending modes are reproduced with frequency differences below 5.6% and MAC numbers over 0.93 for the first two. The torsion mode, which contribution is expected to be significant given the obliquity of the deck and eccentricity of the tracks is specially well calibrated. The fourth and fifth modes present very close frequencies, near 24 Hz and a less accurate adjustment is achieved in these cases. It should be highlighted at this point that only the first span of the bridge was monitored for inaccessibility reasons at the site.

Bridge component	Notation	Initial value	Sensitivity Analysis range	Optimisation range	Final value	Unit	Source
Rail UIC60	E_r	$2.10 \cdot 10^{11}$	-	-	$2.10 \cdot 10^{11}$	Pa	[43]
	I_{yr}	$3038 \cdot 10^{-8}$	-	-	$3038 \cdot 10^{-8}$	m^4	[43]
	m_r	60.34	-	-	60.34	kg/m	[43]
Rail pads	K_p	$1.00 \cdot 10^8$	-	-	$1.00 \cdot 10^8$	N/m	[44]
	C_p	$7.50 \cdot 10^4$	-	-	$7.50 \cdot 10^4$	Ns/m	[45]
Sleepers	E_{sl}	$3.60 \cdot 10^{10}$	-	-	$3.60 \cdot 10^{10}$	Pa	[46]
	ν_{sl}	0.3	-	-	0.3	-	[46]
	w_{sl}	0.30	-	-	0.30	m	[46]
	l_{sl}	2.60	-	-	2.60	m	[46]
	h_{sl}	0.24	-	-	0.24	m	[46]
	M_{sl}	320	-	-	320	kg	[46]
	d_{sl}	0.6	-	-	0.6	m	[46]
Ballast	h_b	0.32	-	-	0.32	m	[37]
	$\boldsymbol{E_b}$	$1.10 \cdot 10^8$	$[-30, +30]\%$	$[-30, +30]\%$	$1.10 \cdot 10^8$	Pa	[45]
	ν_b	0.3	-	-	0.3	-	[47]
	$\boldsymbol{\rho_b}$	1800	$[-30, +30]\%$	$[-30, +30]\%$	1806	kg/m^3	[9]
Degraded ballast	$\boldsymbol{E_{bX}}$=$\boldsymbol{E_{bY}}$	$1.10 \cdot 10^8$	$[-30, +30]\%$	$[-30, +30]\%$	$9.23 \cdot 10^7$	Pa	
	E_{bZ}	$1.10 \cdot 10^8$	$[-30, +30]\%$	-	$1.10 \cdot 10^8$	Pa	[12]
	G_{bYZ}=G_{bXZ}	$4.23 \cdot 10^7$	$[-30, +30]\%$	-	$4.23 \cdot 10^7$	Pa	[12]
	ν_{bXY}=ν_{bYX}	0.2	-	-	0.2	-	[12]
	ν_{bXZ}=ν_{bYZ}	0.2	-	-	0.2	-	[12]
	$\boldsymbol{\rho_b}$	1800	$[-30, +30]\%$	$[-30, +30]\%$	1806	kg/m^3	[9]
Subgrade	E_f	$9.00 \cdot 10^7$	-	-	$9.00 \cdot 10^7$	Pa	[45]
	ν_f	0.3	-	-	0.3	-	[48]
	ρ_f	1800	-	-	1800	kg/m^3	[48]
Girders	$\boldsymbol{E_g}$	$3.74 \cdot 10^{10}$	$[-20, +20]\%$	$[-20, +20]\%$	$4.32 \cdot 10^{10}$	Pa	[49]
	ν_g	0.2	-	-	0.2	-	[49]
	$\boldsymbol{\rho_g}$	$2.23 \cdot 10^3$	$[-8, +8]\%$	$[-8, +8]\%$	$2.23 \cdot 10^3$	kg/m^3	[38]
Slabs	$\boldsymbol{E_s}$	$3.19 \cdot 10^{10}$	$[-20, +30]\%$	$[-20, +30]\%$	$2.55 \cdot 10^{10}$	Pa	[49]
	ν_s	0.2	-	-	0.2	-	[49]
	$\boldsymbol{\rho_s}$	$2.50 \cdot 10^3$	$[-8, +8]\%$	$[-8, +8]\%$	$2.50 \cdot 10^3$	kg/m^3	[49]
Diapraghms	E_{dph}	$2.55 \cdot 10^{10}$	$[-20, +30]\%$	-	$2.55 \cdot 10^{10}$	Pa	[49]
	ν_{dph}	0.2	-	-	0.2	-	[49]
	ρ_{dph}	$2.50 \cdot 10^3$	-	-	$2.50 \cdot 10^3$	kg/m^3	[49]
Handrails	m_b	50	-	-	50	kg/m	
Sidewalks	ρ_f	195	-	-	195	kg/m	[38]
Vertical elastic bearing	E_{eb}	$2.57 \cdot 10^7$	-	-	$2.57 \cdot 10^7$	Pa	[38]
	ν_{eb}	0.49	-	-	0.49	-	[50]
	ρ_{eb}	1230	-	-	1230	kg/m^3	[50]
	$\boldsymbol{R_{eb}}$	1.25	$[0, +60]\%$	$[0, +60]\%$	1.83236	-	
	w_{eb}	0.40	-	-	0.40	m	[38]
	l_{eb}	0.33	-	-	0.33	m	[38]
	h_{eb}	0.049	-	-	0.049	m	[38]
Transverse elastic bearing	K_{eb}	$2.95 \cdot 10^7$	-	-	$2.95 \cdot 10^7$	N/m	[50]
	R_{ebt}	1.25	$[0, +60]\%$	-	1.83236	-	

Table 1: Model parameters: initial values, ranges of variation and final values. Bold letters: parameters included in the optimisation process.

Mode (i)	1	2	3	4	5
f_i^{exp} (Hz)	6.30	7.20	9.30	24.00	24.50
f_j^{num} (Hz)	6.19	6.80	9.79	18.39	24.92
e_{ij} [100%] (-)	1.70	5.51	-5.31	23.35	-1.72
MAC_{ij} (-)	0.93	0.96	0.88	0.79	0.57

Table 2: Experimental and numerical frequencies for modes under 30Hz. Frequency differences and MAC numbers of the paired modes after calibration.

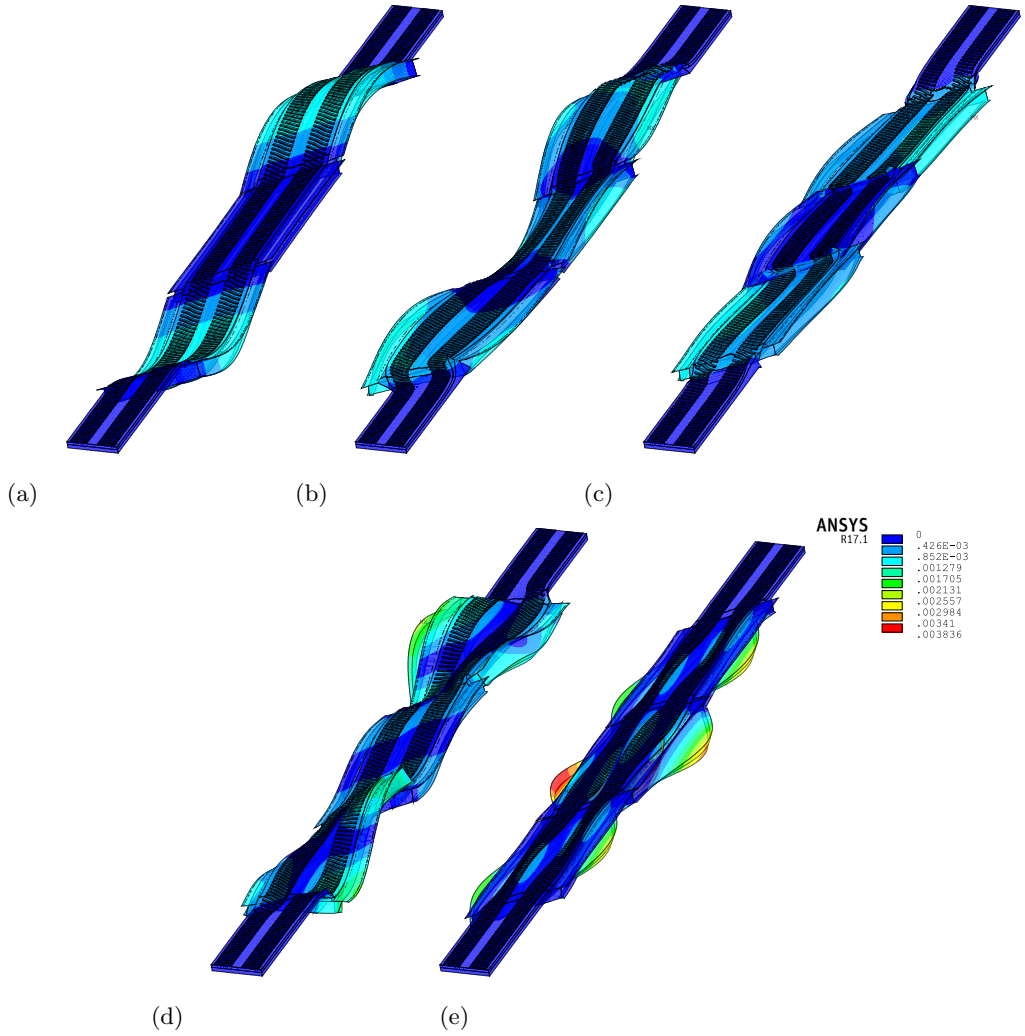

Figure 7: Paired numerical mode-shapes of the calibrated 3D model normalized to the mass matrix. (a) $f_1^{num} = 6.19$ Hz, (b) $f_2^{num} = 6.80$ Hz, (c) $f_3^{num} = 9.79$ Hz, (d) $f_4^{num} = 18.39$ Hz and (e) $f_5^{num} = 24.92$ Hz

4. Sensitivity analysis

In what follows, a comprehensive sensitivity analysis is presented on three geometrical features: (i) the skew angle; (ii) the transverse diaphragms configuration and (iii) the number of spans. The aim is to evaluate the influence of these properties and their combinations on the modal properties and on the maximum vertical response of the bridge under train passages. In what follows, the updated bridge properties (Table 1) are considered as reference case. 25 points of postprocess are defined (see Figure 8) located underneath the girders and uniformly distributed. In sections 4.1 and 4.2 bridges with only one span including the track extension on both sides are considered, while in section 4.3 the influence of the number of spans on the bridge response is investigated.

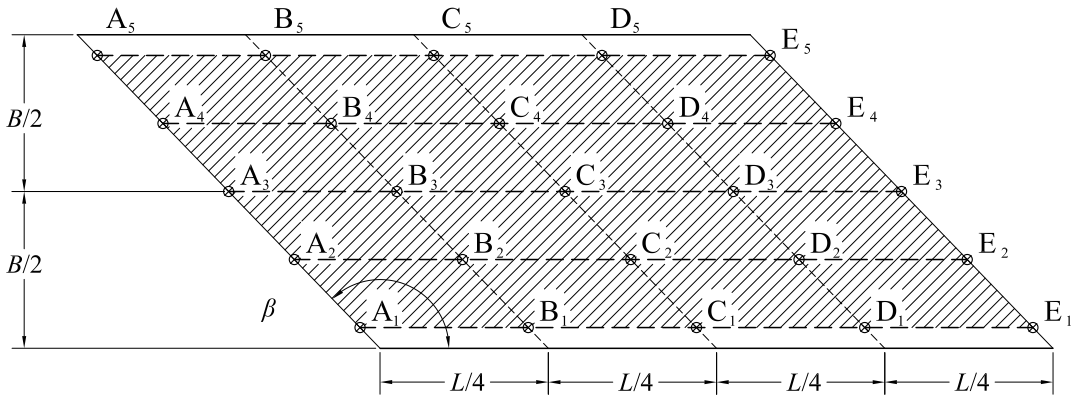

Figure 8: Postprocess points for sensitivity analyses.

4.1. Effect of deck obliquity and diaphragm configuration on the modal parameters

In this subsection, the combined effect of the deck obliquity and the transverse diaphragms configuration on the bridge modal parameters is investigated. Three possibilities are considered based on real scenarios that can be found in existing girder bridges: (i) cast-in-place concrete diaphragms fully connected to the girders web, top flange and upper slab (FD); (ii) poorly built diaphragms connected to the girders web but not to the upper slab (PD); absence of diaphragms (ND). The combined influence of these restraining elements and the deck skewness is evaluated on the frequency differences and MAC numbers of the first three modes, considering the case with one span, full diaphragms and straight deck ($\beta = 90°$) as reference.

In Figure 9 the MAC and frequency differences $\bar{e}_{ii}$ for the i-*th* mode are represented versus β for three diaphragm configurations, where $\bar{e}_{ii}$ is computed here as per,

$$\bar{e}_{ii}\,[100\%] = \frac{f_{i,\beta}^{\mathrm{XD}} - f_{i,\beta=90°}^{\mathrm{FD}}}{f_{i,\beta=90°}^{\mathrm{FD}}} \cdot 100 \tag{5}$$

$$\mathrm{MAC}_{ii} = \frac{\left(\Phi^{\mathrm{XD}}_{i,\beta} \cdot \Phi^{\mathrm{FD}}_{i,\beta=90^\circ}\right)^2}{\left(\Phi^{\mathrm{XD}}_{i,\beta} \cdot \Phi^{\mathrm{XD}}_{i,\beta}\right) \cdot \left(\Phi^{\mathrm{FD}}_{i,\beta=90^\circ} \cdot \Phi^{\mathrm{FD}}_{i,\beta=90^\circ}\right)} \tag{6}$$

where X refers to the fully connected (F), poorly built (P) or absence (N) of diaphragms. The MAC is computed using the 25 postprocess points, applying Equation 6 between the straight FD reference model and each of the 36 cases evaluated (3 diaphragm configurations $\times$ 12 β values). The first longitudinal bending

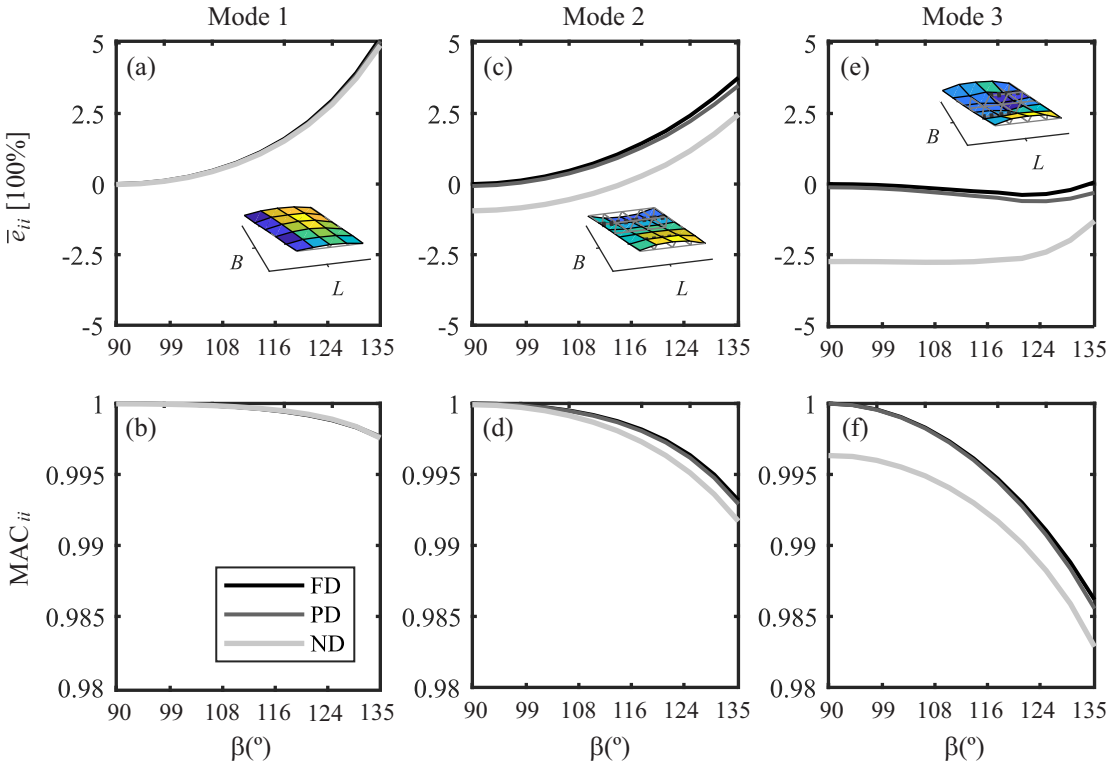

Figure 9: Frequency differences and MAC values with respect to reference case for FD (full diaphragms), PD (partial diaphragms) and ND (no diaphragms) models versus deck skewness.

mode is the least affected by the transverse diaphragms, even in the case of highly skewed bridges. However, the fundamental frequency is the one most affected by the skew angle, increasing in approximately 5% in the most oblique case. The second (first torsion) natural frequency also increases with this parameter but to a less extent, and the third (first transverse bending) natural frequency remains almost unaffected by the deck obliqueness. The presence of the transverse diaphragms increases the second (first torsion) and third (first transverse bending) natural frequencies in a similar proportion for all the levels of skewness considered. The alteration in the modal shapes is small, being the third mode the one most affected. Finally, the full and monolithic connection of the transverse diaphragms to the slab (FD vs. PD cases) has no apparent effect on the bridges modal parameters.

4.2. Effect of deck obliquity and diaphragm configuration on the maximum acceleration under train passages

In what follows the dynamic response of one-span bridges with different levels of skewness and transverse diaphragm configurations is analysed under the circulation of the 10 trains from the High Speed Load Model-A (HLSM-A) from EC1. The trains cross the bridge along track 2 (see Figure 3) at constant speeds in the X positive direction. The speed range considered is $[144 - 421.2]$ km/h in 3.6 km/h increments. 9 bridge models are evaluated: three levels of obliquity ($\beta = [90, 112, 134]^\circ$) and the previous diaphragms cases (FD, PD and ND). As indicated in Section 3.1, the dynamic problem is solved by Modal Superposition in the time domain. In this section only the contribution of the first three modes of vibration (first longitudinal bending, first torsion and first transverse bending modes) is considered, and a modal damping ratio of 1% is admitted as recommended in [9] for the particular material and span length. Finally, envelopes of maximum acceleration $|a_{max}|$ at the 25 points of postprocess are computed. In Table 3 the maximum acceleration reached in each of the 9 cases of study is included, along with the postprocess point, the train and the speed.

Diaphragm conf.	$\lvert a_{max}\rvert$ (m/s^2)	$\beta = 90^\circ$	$\beta = 112^\circ$	$\beta = 134^\circ$
FD	Value	4.322	4.189	3.234
	Point (Figure 8)	C2	C2	C1
	Train/V(km/h)	A3/421.2	A3/421.2	A10/396.0
PD	Value	4.312	4.186	3.343
	Point (Figure 8)	C2	C2	C1
	Train/V(km/h)	A3/421.2	A3/421.2	A10/396.0
ND	Value	4.333	4.130	3.580
	Point (Figure 8)	C2	C2	C1
	Train/V(km/h)	A3/421.2	A3/421.2	A10/392.4

Table 3: Maximum vertical acceleration, postprocess point, train and travelling speed for $\beta = [90, 112, 134]^\circ$ and diaphragm configurations FD, PD and ND.

The overall maximum acceleration reaches 4.33 m/s^2, higher than the limit prescribed in EC [6] for ballast track bridges 3.5 m/s^2. Nevertheless, the design speed considered corresponds to a maximum speed in the railway line section of 350 km/h, which exceeds the actual one (300 km/h). For the decks with $\beta = 90^\circ$ and $\beta = 112^\circ$ train HSLM-A3 induces the maximum acceleration at the maximum speed considered and at point C2, under the loaded track. This is due to the excitation of first resonance of the fundamental mode. In the bridges with $\beta = 134^\circ$ this resonant speed falls out of the speed window of analysis and the maximum acceleration happens at C1 (border girder) under the circulation of HSLM-A10 train, which excites second resonance of the torsion mode at 396 km/h. The theoretical resonant speeds for these two trains in the FD

case are given by

$$V_{i=1,j=1}^{rA3,90^\circ} = \frac{d \cdot f_1 \cdot 3.6}{j} = \frac{20\text{m} \cdot 5.83\,\text{Hz} \cdot 3.6}{1} = 419.8\,\text{km/h} \tag{7a}$$

$$V_{i=2,j=2}^{rA10,134^\circ} = \frac{d \cdot f_2 \cdot 3.6}{j} = \frac{27\text{m} \cdot 8.15\,\text{Hz} \cdot 3.6}{2} = 395.9\,\text{km/h} \tag{7b}$$

where d stands for the characteristic distance between repeated axle loads. In Figure 10 envelopes of maximum acceleration for the 10 HSLM-A trains and for the complete range of velocities are represented at the 25 postprocess points. A-E defines the cross section and 1-5 the particular point (see Figure 8). Figures (a), (b) and (c) correspond to skew angles of 90°, 112° and 134°, while light grey, dark grey and black stand for the three diaphragm configurations FD, PD and ND, respectively. From the analysis of the figure it can be concluded that (i) the overall maximum acceleration reduces in general with the deck obliqueness; (ii) the overall maximum response always takes place at mid-span, consistently with the modes accounted for in the analysis; (iii) in straight bridges or bridges with small obliqueness, the influence of the diaphragm configuration is negligible. However, for relevant levels of skewness, decks without transverse diaphragms exhibit higher vertical accelerations at the border girders, especially if the participation of the torsion mode is significant, as it is in this case.

Finally, in Figure 11 envelopes of maximum acceleration for the 10 HSLM-A trains at point C1 are plotted in terms of the circulating velocity accounting for a different number of modal contributions: the first column plots (a-c) are obtained accounting for the participation of the fundamental mode; while the second and third column plots account for the contribution of the first and second (d-f), and the first three modes (g-i), respectively. In each subplot, light grey, dark grey and black traces correspond to the response computed for the diaphragm configurations FD, PD and ND, respectively. Associated to some of the resonant peaks, the train causing resonance, the mode under resonance (i) and the resonance order (j) are specified in Figure 11(g) with the nomenclature ATr(i,j), for Tr being the train number. It is concluded that (i) the contribution of modes different from the longitudinal bending one is very relevant for speeds higher than 300 km/h in all the cases. This is related to second resonances ($j = 2$) of the torsion mode ($i = 2$) excited by the trains with longest characteristic distances A7 to A10. This shows the importance of the use of structural models that not only account for the longitudinal bending of the bridge; (ii) the contribution of the transverse bending modes is visible only for the highest obliquity level; (iii) the resonant speeds vary consistently with the evolution of the natural frequencies shown in Figure 9; (iv) the overall maximum acceleration reduces with the skew angle mainly because the first resonance of the fundamental mode falls out of the speed window in the case $\beta = 134^\circ$, due to the increase in the fundamental frequency; (v) the influence in the diaphragm configuration (FD vs PD) is negligible on the maximum acceleration, no matter the bridge obliqueness. Nevertheless, the total absence of these elements (ND) is relevant in oblique cases, leading to an increment in the maximum acceleration of approximately 10% in the cases evaluated.

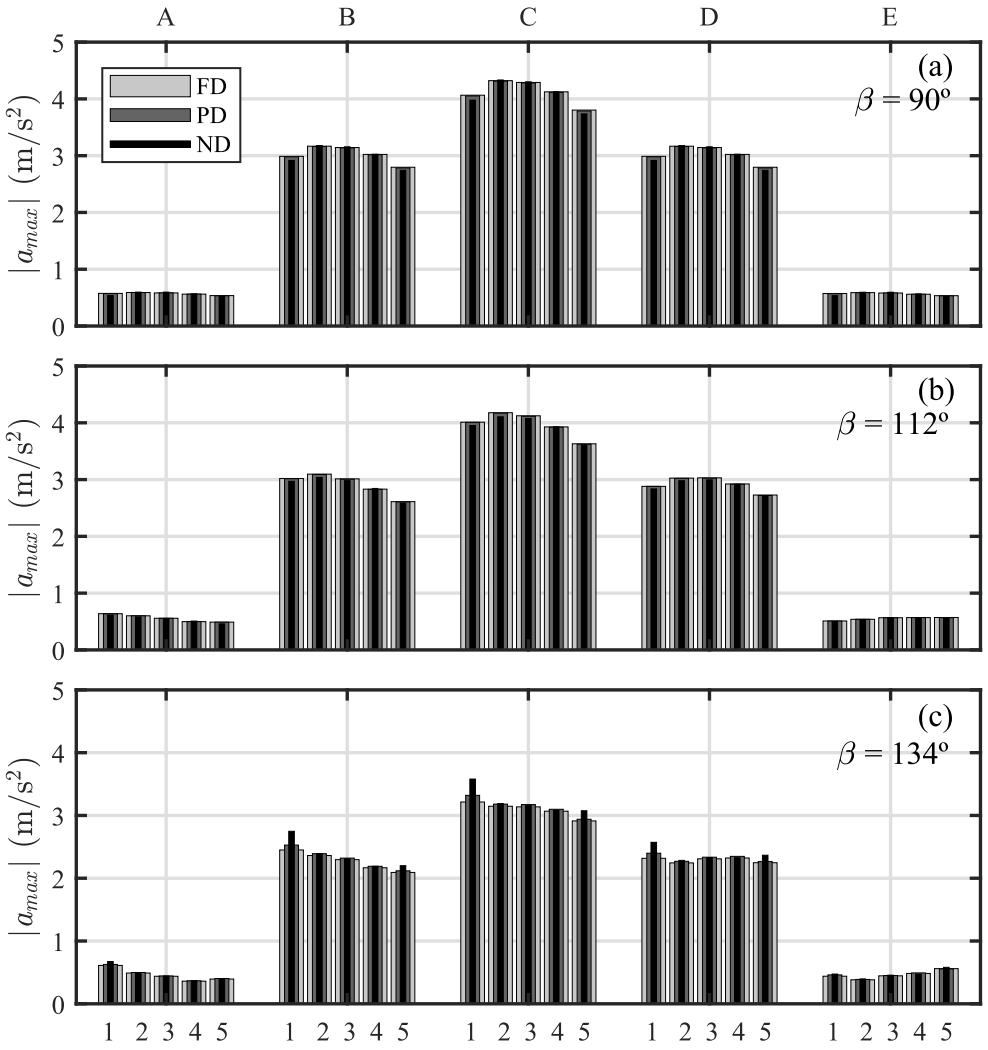

Figure 10: Maximum acceleration at postprocess points (Figure 8) under HLSM-A trains in the speed range $[144-421.2]$ km/h. Thickest bars in light gray, FD; medium width bars in dark gray, PD; and thinnest black bars ND.

4.3. Effect of the number of spans on the maximum acceleration under train passages

In this section the effect of the number of spans structurally independent but weakly connected through the degraded ballast layer is investigated. 18 bridge models are designed to this end considering the previous levels of skewness (90°, 112° and 134°), the presence or absence of diaphragms (FD and ND) and either 1, 2 or 3 spans. The diaphragm configuration PD is not evaluated in this section due to its negligible influence on the maximum acceleration when compared to FD. In all the cases the properties are those of the Jabalón Bridge updated model and the 15 m track extension is included on each side of the bridges.

As in the previous section, the bridge response is obtained by Modal Superposition of the first 3 modes under the HSLM-A trains in the speed range $[144-421.2]$ km/h in 3.6 km/h increments. In bridges with 1, 2 and 3 spans the maximum vertical response is obtained at 25, 50 and 75 points, respectively. The

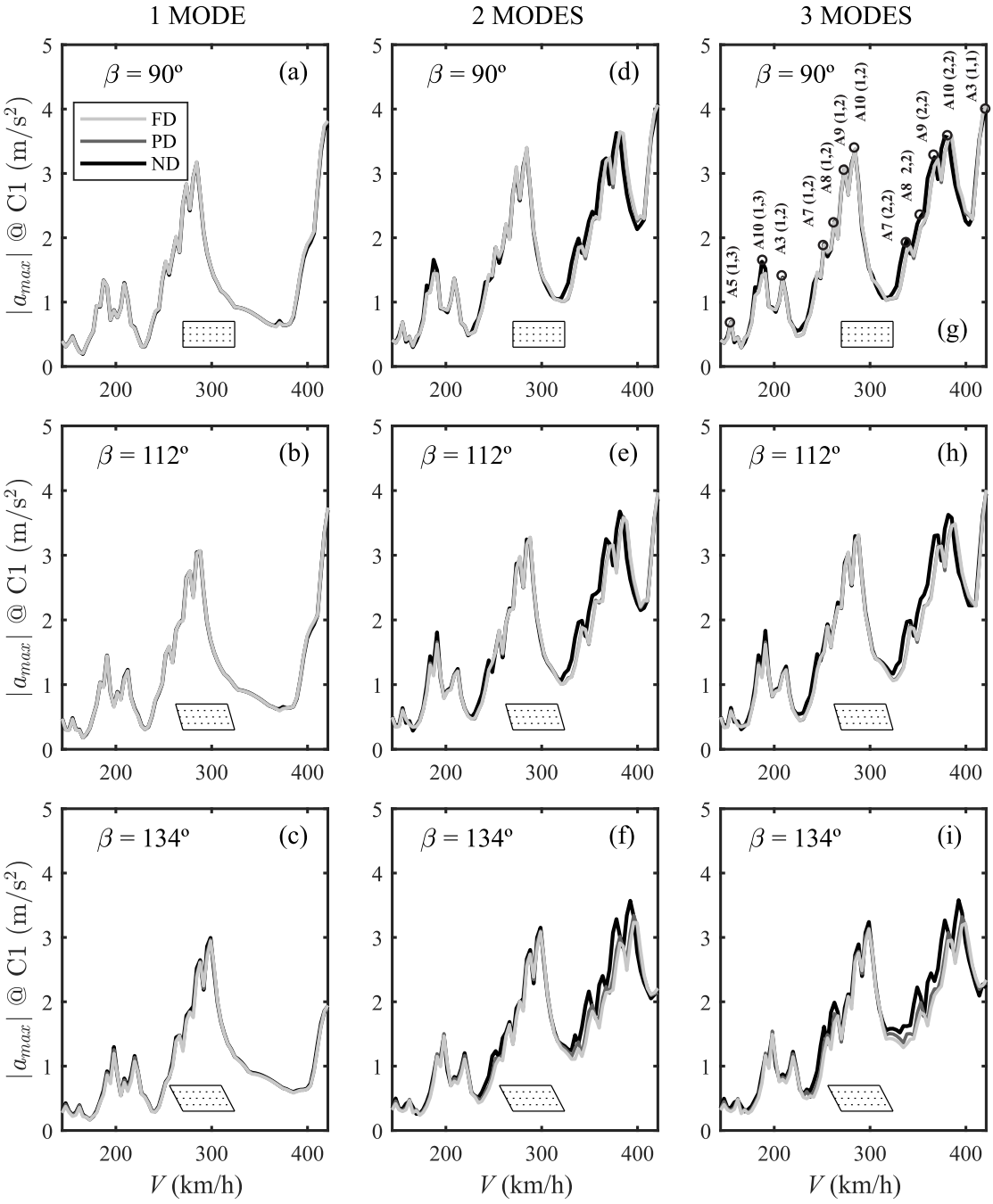

Figure 11: Maximum acceleration at C1 under passage of HLSM-A trains in the speed range $[144-421.2]$ km/h.(a,d,g) $\beta = 90°$; (b,e, h) $\beta = 112°$ and (c,f, i) $\beta = 134°$, considering the contribution of (a-c) only the fundamental mode, (d-f) first and second modes and (g-i) the first three modes.

postprocess points are distributed in each span as shown in Figure 8. Labels A-E, F-J and K-O identify these points in the first, second and third span, respectively; span 1 being always the first span in the

travelling direction.

In what follows an acceleration amplification ratio $\bar{a}_{max}$ is defined as the quotient between the maximum acceleration predicted for the 10 trains in the complete range of velocities at a particular postprocess point (P) and the overall maximum acceleration provided by the single-span model for the same set of trains and velocities throughout all the postprocess points:

$$\bar{a}_{max} = \frac{|a_{max}(P)|}{|max(a_{max}^{N_{sp}=1})|} \tag{8}$$

In Figures 12 and 13, $\bar{a}_{max}$ is represented at the postprocess points in the two-span and three-span bridges. Notice that values standing above the dashed line indicate that the response predicted by the two or the three-span models exceeds the overall maximum acceleration predicted by the single-span model. Solid columns correspond to decks with full diaphragms (FD) and white columns to decks with no diaphragms (ND). Notice that in Equation 8 numerator and denominator refer to the same type of deck in terms of obliqueness and diaphragm configuration. The same ratio in terms of vertical displacement $\bar{d}_{max}$ is computed but homologous representations are not included for the sake of conciseness. From this analysis it is concluded that for the analysed configurations the maximum acceleration predicted by one-span models is superior to that predicted by two-span models, both in terms of displacements and of accelerations, independently on the skewness and diaphragm configuration. In three-span models the maximum response is predicted at the central span, with a maximum exceedance of the one-span model predictions of 27% in accelerations and of 17% in the case of displacements. This confirms previous results by the authors [51, 52] and indicates that one-span models may not always be on the safe side when assessing the maximum dynamic response of multi-span SS railway bridges. Particularly, in reference [52] it was observed that the maximum response can be found in different spans depending on several factors such as the span length and the relative flexibility of the bridges and the elastic supports. Further research is needed in order to clarify under what circumstances single-span models may not predict the overall maximum acceleration of multi-span railway bridges weakly connected through the ballast track.

For moderate skew angles, similar $\bar{a}_{max}$ and $\bar{d}_{max}$ distributions are obtained for FD and ND cases. For the most oblique bridges, i.e. $\beta = 134°$, the overprediction of the response provided by FD bridges is higher than in the ND case, especially at the central span deck borders. This has to do with the fact that the numerator in Equation 8 is approximately the same for FD and ND models but the denominator is higher in the absence of diaphragms, as already shown in Figure 10.

5. Numerical-experimental comparison in Jabaln Bridge under operating conditions

During the experimental campaign performed on Jabalón Bridge the vertical response was registered under several HS train circulations. In this section the vertical acceleration at the sensors indicated in

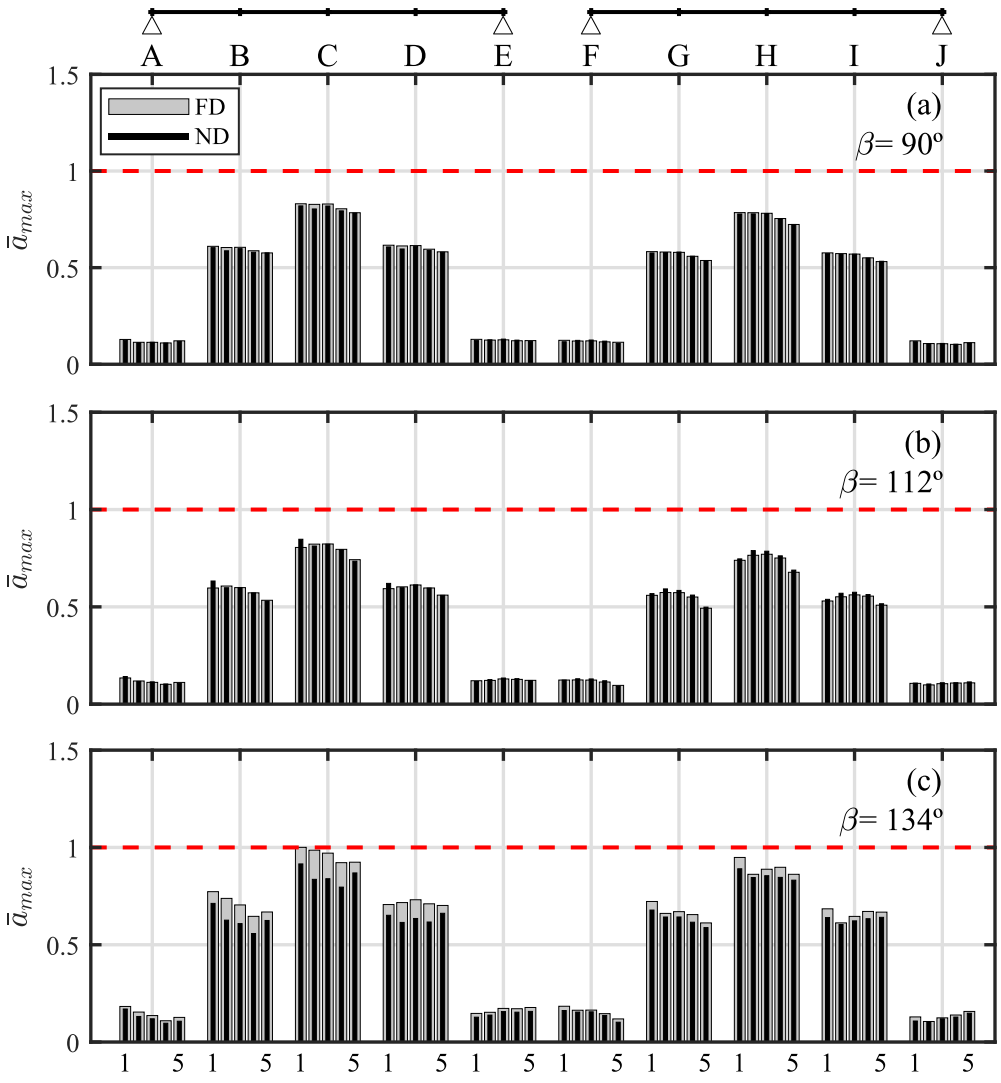

Figure 12: Amplification acceleration $\bar{a}_{max}$ ratio at each bridge postprocess point considering models with two spans (points $A_1 - A_5$ to $J_1 - J_5$). Thickest bars in light gray, FD; thinnest black bars, ND.

Figure 3 installed underneath the girders lower flange is included for two of these train passages (RENFE S102 and S104 trains), and a numerical–experimental comparison is presented. The two particular passages are selected as neither of them induce a relevant resonance of the bridge fundamental mode. For this reason, several modal contributions different from the longitudinal bending one contribute to the acceleration response, and the interaction of the bridge with the trains suspension systems is not expected to be relevant at the fundamental frequency.

RENFE S102 is a regular Talgo train composed of two locomotives and 12 passenger coaches. The

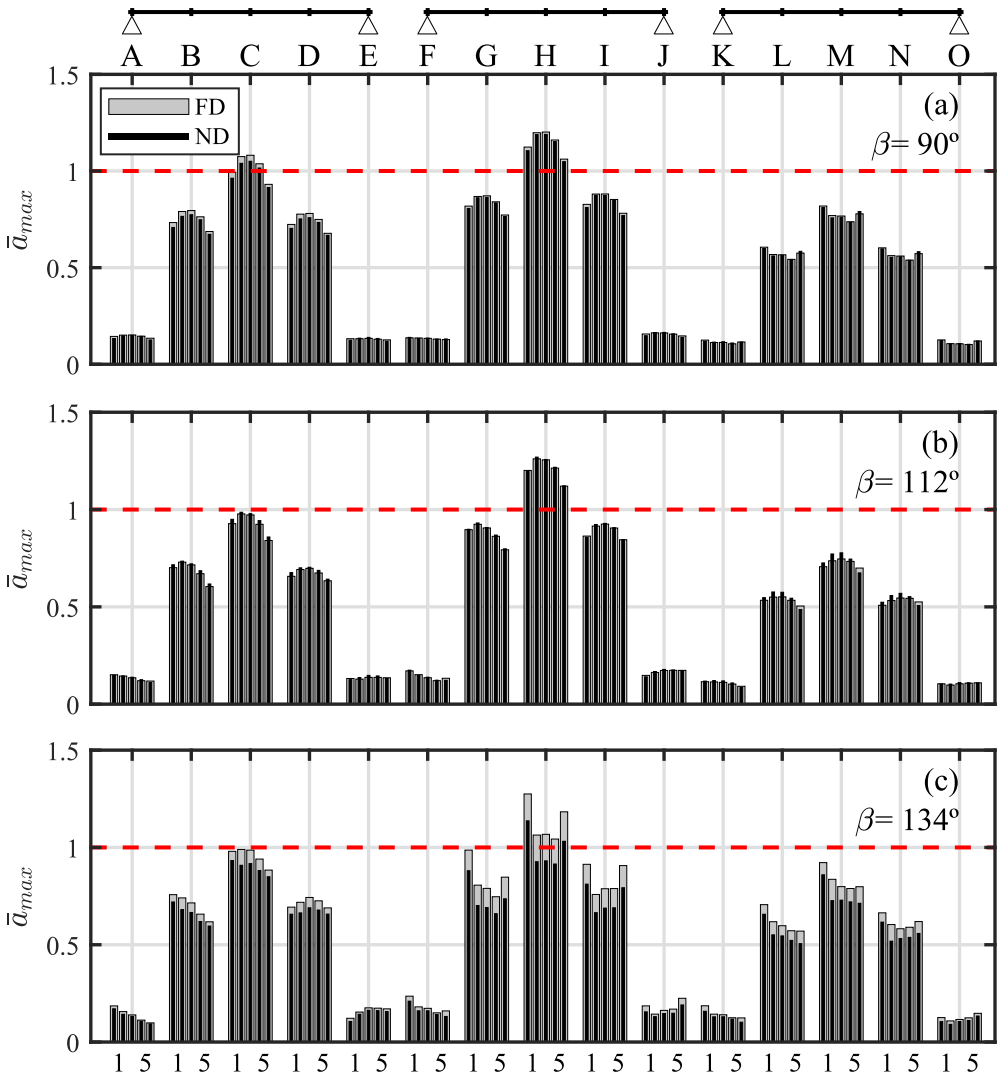

Figure 13: Amplification acceleration $\bar{a}_{max}$ ratio at each bridge postprocess point considering models with three spans (points $A_1 - A_5$ to $J_1 - J_5$). Thickest bars in light gray, FD; thinnest black bars, ND.

distance between shared axles in the passenger coaches of this train is $d = 13.14\,\text{m}$. On the other hand, RENFE S104 is a conventional train with distributed traction composed of two locomotives and two passenger coaches. In this case the distance between the front or the rear bogies of consecutive coaches is $d = 25.9\,\text{m}$. These characteristic distances may induce resonance of the lowest modes of the bridges, given the train speeds and bridge natural frequencies. In Table 4 the track number, travelling direction (M: Madrid, S: Sevilla), coaches configuration (L: locomotive, C: carriage), circulating speed and the axles scheme and load values are included. For more details about the train configurations the reader is referred to Reference

[32].

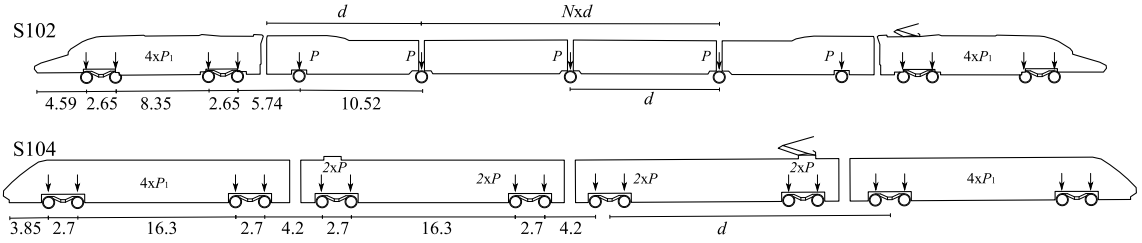

Train	Track	Ride	Scheme	V (km/h)	N	d (m)	P_1 (kN)	P (kN)
S102	1	M-S	L-12C-L	240	12	13.14	170	[156-170]
S104	1	M-S	L-2C-L	249	2	25.9	153	[153-153]

Table 4: RENFE S102 and S104 train passages information.

In Figures 14 and 15 the vertical acceleration under the passages of S102 and S104 trains at the locations of four accelerometers is represented. In the first case, selected accelerometers are $01z$ and $03z$, located at the border girder closest to the loaded track, and 07z and 09z, located underneath the girders #1 and #2, at the unloaded track side of the deck. In the second case accelerometers $01z$, $03z$, $05z$ and $15z$ are the ones represented, $15z$ being installed under girder #4, very close to the Sevilla abutment. In both figures the acceleration is plotted in the time domain (first column), frequency domain (second columns) and in one-third octave frequency bands (third column). Experimental results are represented in black trace, and numerical predictions in red and gray traces. The frequency domain results are obtained performing a Fast Fourier transform (FFT) on the experimental and on the numerical data using Matlab. Consequently, the amplitude of the peaks is proportional to the sample size and the sampling rate of the discrete signal. Therefore, to allow the comparison between the amplitude peaks from the experimental signal and those from the numerical predictions, as a previous step to perform the FFT, the numerical responses have been resampled to the sampling rate of the experimental signal to achieve comparable peak amplitudes between the different curves shown in the figures.

Regarding the numerical predictions, two numerical responses are superimposed: in red trace, the one obtained with the updated model of Jabalón Bridge with three spans (section 3.2); and in grey trace, the response is calculated with the same model but ignoring the deck obliquity (i.e. $\beta = 90°$). The fundamental frequency predicted by these two models are 6.19 Hz and 5.91 Hz for the skew and straight cases, respectively. The bridge vertical response under the train passages is obtained by Modal Superposition considering the contribution of modes under 30 Hz. Modal damping values identified from the free vibrations left by the trains and included in Figure 4 are assigned to the paired modes (and to homologous modes in the straight model) and 1% is assigned to the remaining ones according to EC [9]. The experimental response is filtered applying two third-order Chebyschev filters with high-pass and low-pass frequencies of 1 Hz and 30 Hz,

respectively.

S102 train is characterised by a high number of axles and a short characteristic distance d. For this reason it may induce resonance on a bridge at a lower speed than other trains with longer coaches lengths. In this particular case the train velocity falls in between the first and second theoretical resonant velocities of the fundamental mode given by $V_{1,1}^{rS102} = f_1^{exp} \cdot d/1 = 298\,\text{km/h}$ and $V_{1,2}^{rS102} = f_1^{exp} \cdot d/2 = 149\,\text{km/h}$. The second (first torsion) and third (fist transverse bending) modes do not undergo resonance either under this train at the particular velocity. The overall maximum acceleration registered in the first span under the passage of S102 reaches $0.75\,\text{m/s}^2$ and is detected at accelerometer 02z. In Figures 14(e)-(f) the response of the bridge in the frequency domain is presented. Several frequency contributions affect the vertical response of the bridge. Clearly the deck behaviour differs from that of a beam-type structure. The peak associated to the axle distance $V/d = 5.07\,\text{Hz}$ is well fitted, meaning that the travelling speed was correctly identified. Peaks at multiples of this frequency are clearly visible in the spectrum, especially at the accelerometers located under the loaded track. The contribution of the deck torsion mode with identified natural frequency 7.2 Hz is relevant especially at the $03z$, $07z$ and $09z$ sensors, close to the deck border.

Regarding the numerical-experimental comparison, and focusing on the response predicted by the updated skewed model, peaks associated to the bridge modes under $[20-25]\,\text{Hz}$ are reasonably well reproduced. The response in the $[25-30]\,\text{Hz}$ frequency band is under-predicted by the numerical model, which probably is related to the fact that track irregularities are neglected. As resonances of the lowest modes are not induced in this case, VBI effects are less relevant. As a result, the numerical model does not over-predict the experimental response at low frequencies. The free vibration response is well fitted which is expectable, as damping has been identified from the free vibrations left by the trains. Finally, the numerical response predicted by the straight 90° numerical model is compared to the experimental response. Clearly this model leads to an overprediction of the accelerations in the complete frequency band when compared to the 134° model, with the exception of the very low frequencies. In fact, the bogie passing frequency amplitude is well represented. Nevertheless, the frequency amplitudes related to the bridge first natural modes are clearly overpredicted with the straight model. This is consistent with the results presented in section 4.2 and Table 3, where the maximum acceleration under the HSLM-A trains is calculated for different skew angles and diaphragm configurations, considering the contribution of the first 3 modes. In addition to this, in the particular case shown in Figure 14, the straight model also leads to considerably higher accelerations in the $[12-20]\,\text{Hz}$ frequency band, which may be related to modes which were not identified during the experimental campaign. The differences between the two models diminish close to the 30 Hz limit.

Focusing now on Figure 15, which represents the numerical-experimental comparison of the bridge response under the S104 train, the maximum acceleration in this case is detected at sensor 11z and reaches $1\,\text{m/s}^2$. Again, this train axle scheme and travelling velocity do not induce resonance of any of the first three modes identified under ambient vibration. The second and third resonance velocities of the first, second

and third modes are theoretically $V_{1,2}^{rS104} = f_1^{exp} \cdot d/2 = 294\,\text{km/h}$ and $V_{1,3}^{rS104} = f_1^{exp} \cdot d/3 = 196\,\text{km/h}$ for the fundamental mode, $V_{2,2}^{rS104} = f_2^{exp} \cdot d/2 = 336\,\text{km/h}$ and $V_{2,3}^{rS104} = f_2^{exp} \cdot d/3 = 224\,\text{km/h}$ for the torsion mode and $V_{3,2}^{rS104} = f_3^{exp} \cdot d/2 = 433.6\,\text{km/h}$ and $V_{3,3}^{rS104} = f_3^{exp} \cdot d/3 = 289\,\text{km/h}$ for the transverse bending mode, which are distant from the actual speed of 249 km/h. The resonant speeds are higher than in the S102 case due to the longer characteristic distance of S104.

In the frequency domain plots, Figure 15(e)-(h), the numerical response given by the updated skewed model (in red trace) matches the bogie passing frequency ($V/d = 2.67\,\text{Hz}$). The numerical-experimental fitting up to 22 Hz is excellent, both in frequency and in amplitude. The response is well represented even close to the abutment (accelerometer $15z$) which is not easy due to the dependence of the model on the boundary conditions, given the high obliquity of the deck. Again, the contributions of the first transverse and first torsion modes are relevant. This highlights the necessity to use three-dimensional models to properly predict the dynamic response of these oblique double-track girder bridges. The time history response is again correctly predicted under free vibration. Frequency contributions between $[25 - 30]\,,\text{Hz}$ are again underestimated by the skew model. Finally, when the obliquity of the deck is disregarded (grey trace) a clear overprediction of the acceleration happens with a relevant contribution close to 20 Hz.

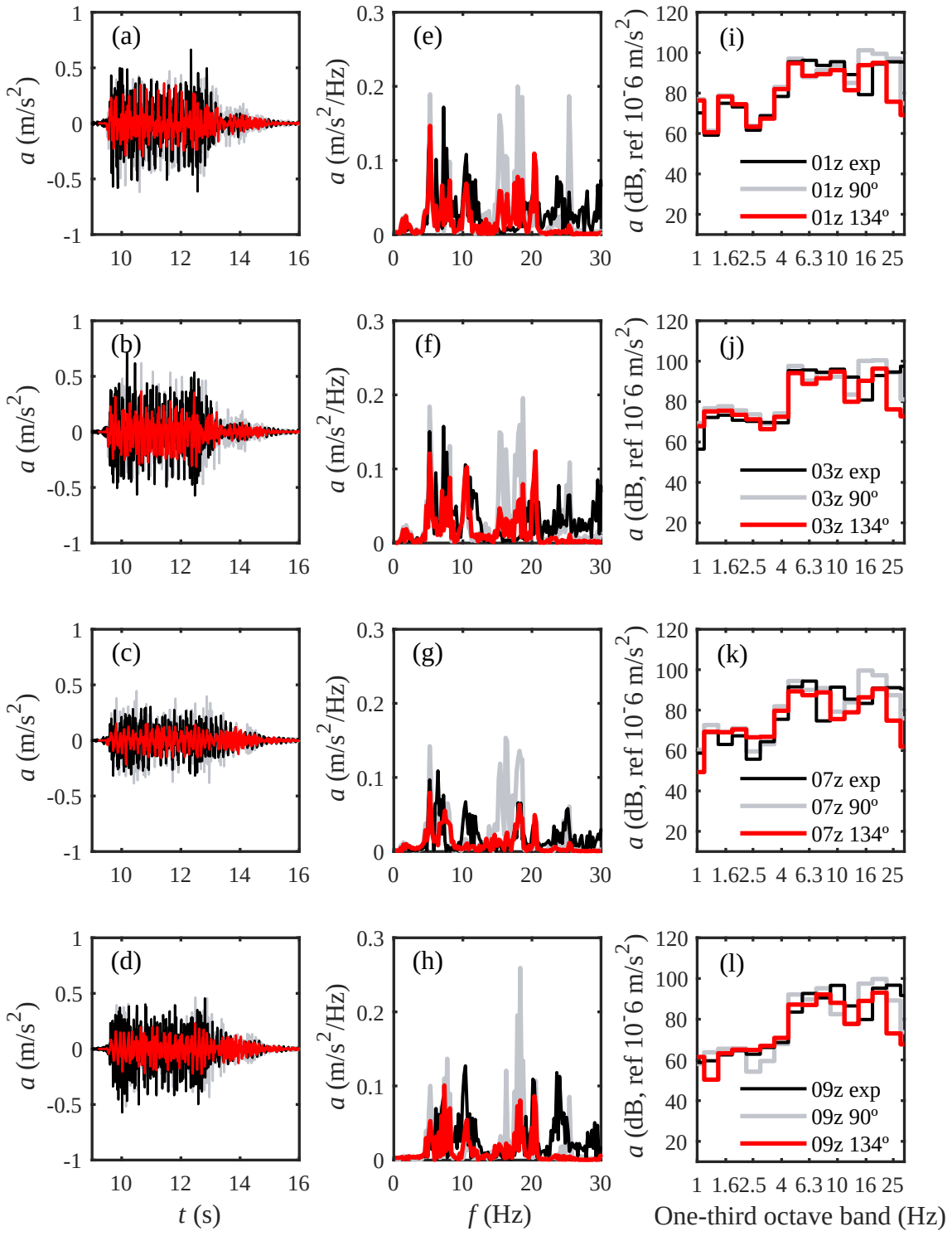

Figure 14: Time history (a-d), frequency content and (e-h) one-third octave band representation of the acceleration (i-l) under RENFE S102 train travelling at 240 km/h on track 1. Experimental results (black trace) vs. numerical predictions: : skew angle $\beta = 90°$ (gray trace); $\beta = 134°$ (red trace).

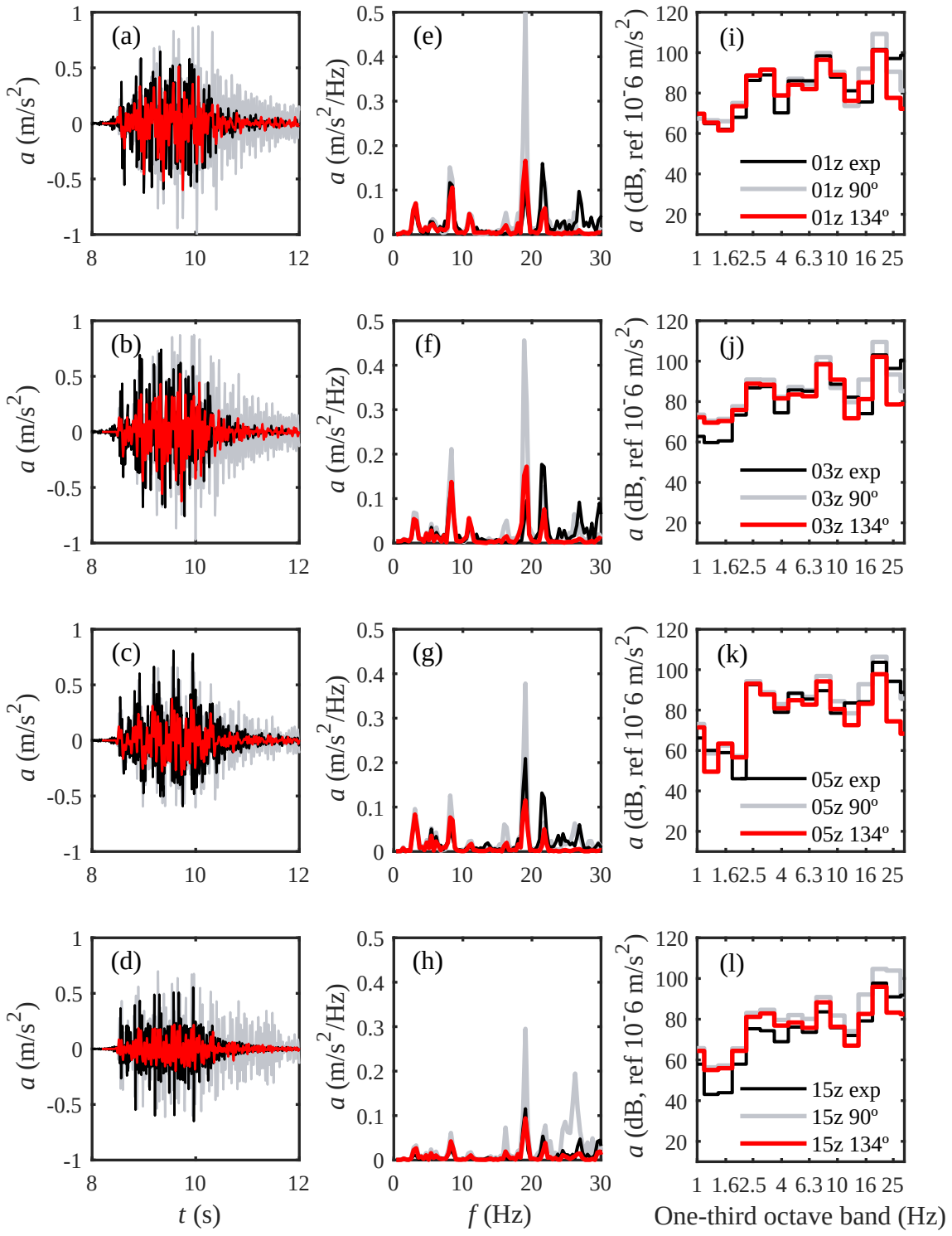

Figure 15: Time history (a-d), frequency content and (e-h) one-third octave band representation of the acceleration (i-l) under RENFE S104 train travelling at 249 km/h on track 1. Experimental results (black trace) vs. numerical predictions: skew angle $\beta = 90°$ (gray trace); $\beta = 134°$ (red trace).

6. Conclusions

In this work the dynamic response of High-Speed multi-track railway bridges composed by simply-supported spans and girder decks is investigated. With the performed analyses the influence and correlation of three geometrical aspects usually disregarded in numerical models used to evaluate the Serviceability Limit State of traffic safety has been evaluated: (i) the deck obliquity, (ii) the presence and correct execution of transverse diaphragms at the supports, and (iii) the number of successive simply-supported spans weakly coupled through the ballast track. To this end 3D detailed FE models of realistic bridges of span lengths close to 25 m are implemented including the ballast track and the possible degradation of the ballast layer between the successive spans.

From the sensitivity analyses performed on the evolution of the modal parameters the following can be concluded:

- All the bridges analysed present the same first three modes of vibration: longitudinal bending, first torsion and first transverse bending modes. The deck obliquity leads to a clear increase of the fundamental mode natural frequency. The second (first torsion) frequency also increases with this parameter but to a less extent, and the third (first transverse bending) natural frequency remains almost unaffected by the deck obliqueness. The alteration of the modal shapes is small in all the cases.

- The fundamental frequency is practically unaffected by the presence of the transverse diaphragms, even in the most oblique cases. The transverse diaphragms lead to an increase of the second and third natural frequencies in a similar proportion for all the levels of skewness considered.

- The full and monolithic connection of the transverse diaphragms to the slab has no apparent effect on the bridges modal parameters. Similar results are obtained with fully connected and partially connected diaphragms throughout the study.

Concerning the maximum response of the bridges under train passages the following is concluded:

- The resonant speeds vary consistently with the evolution of the natural frequencies.

- In the cases analysed, the overall maximum acceleration reduces with the deck obliqueness. Nevertheless, this is mainly caused by the fact that resonances that take place at the highest velocities considered, fall out of the speed window as the deck skewness increases. This not being the case, the detected differences are lower.

- The contribution of modes different from the longitudinal bending one is very relevant for speeds higher than 300 km/h in all the cases analysed. This shows the importance of using structural models that do not only account for the longitudinal bending response of the bridge.

- The influence in the diaphragm configuration (FD vs. PD) is negligible on the maximum acceleration under train passages, no matter the bridge obliqueness. Nevertheless, the total absence of these elements is relevant in oblique cases, leading to an increment in the maximum acceleration of approximately 10% in the cases evaluated.

In relation to the investigation on the number of spans included in the analyses it may be concluded that models with three spans predict the maximum response at the central span, with a maximum exceedance of the one-span model predictions of 27% in accelerations and of 17% in the case of displacements. This indicates that one-span models may not always be on the safe side when assessing the maximum dynamic response of multi-span SS railway bridges. Extending the sensitivity analyses and the investigation on the effect of the number of spans to bridges with different span lengths could be of interest for future investigations, as some of the observed tendencies may aggravate in the case of shorter spans.

As per the numerical-experimental comparison presented in the last section, the response of Jabalón Bridge in terms of accelerations exhibits a noticeable contribution of modes different from the longitudinal bending one. The updated 3D FE numerical model reproduces with reasonable accuracy the bridge response up to 25 Hz, approximately. It should be noted that a moving load model is used and that the effect of irregularities is not accounted for. Also, when neglecting the deck obliquity, the correspondence worsens as excessively high accelerations are predicted. Finally, the proper definition of boundary conditions in these type of SS bridges with an important level of obliquity is essential in order to adequately reproduce the modal properties and the dynamic response. Simplifications admitted in straight decks may not be adequate for high obliquity levels.

Acknowledgements

The authors would like to acknowledge the financial support provided by the Spanish Ministry of Science and Innovation and by Generalitat Valenciana under research projects PID2019-109622RB-C2 and AICO/2021/200. Also, the support provided by Universitat Jaume I through its 2021 institutional research plan is acknowledged (UJI-B2021-16).

References

[1] European Environment Agency, Rail and waterborne - best for low-carbon motorised transport (03-2021).

[2] UIC - International Union of Railways, Rail bridges for speeds > than 200km/h. , Final report. Part A. Synthesis of the results of D214 research ERRI-D-214/RP9.

[3] L. Frýba, Dynamic behaviour of bridges due to high-speed trains, in: Workshop bridges for high-speed railways, Porto, 2004, pp. 137–158.

[4] W. Hoorpah, Dynamic calculations of high-speed railway bridges in France some case studies, in: Taylor & Francis (Ed.), Dynamics of High-Speed Railway Bridges, no. 978-0-203-89540-5, 2008, pp. 133–146.

[5] M. Zacher, M. Baeßler, Dynamic behaviour of ballast on railway bridges, in: Taylor & Francis (Ed.), Dynamics of High-Speed Railway Bridges, no. 978-0-203-89540-5, 2008, pp. 99–112.

[6] CEN/TC250, Eurocode: Basis of structural design. Annex A2: Application for bridges. Final version, European Committee for Standardization, Brussels, 2005.

[7] L. Frýba, Dynamics of railway bridges, Thomas Telford, 1996.

[8] Y.B. Yang, J.D. Yau, L.C. Hsu, Vibration of simple beams due to trains moving at high speeds, Engineering Structures 19 (11) (1997) 936–944.

[9] CEN, EN 1991-2, Eurocode 1: Actions on Structures - Part 2: Traffic loads on bridges, European Committee for Standardization, Brussels, 2002.

[10] K. Nguyen, C. Velarde, J.M. Goicolea, Analytical and simplified models for dynamic analysis of short skew bridges under moving loads, Advances in Structural Engineering 22 (9) (2019) 2076–2088.

[11] L. R. Ticona Melo, D. Ribeiro, R. Calçada, T. N. Bittencourt, Validation of a vertical train-track-bridge dynamic interaction model based on limited experimental data, Structure and Infrastructure Engineering 16 (1) (2020) 181–201.

[12] J.C. Sánchez-Quesada, E. Moliner, A. Romero, P. Galvín, M.D. Martínez-Rodrigo, Ballasted track interaction effects in railway bridges with simply-supported spans composed by adjacent twin single-track decks, Engineering Structures (247) (2021) 113062.

[13] Y. Xiao, X. Luo, J. Liu, K. Wang, Dynamic Response of Railway Bridges under Heavy-Haul Freight Trains, Advances in Civil Engineering 2020 (2020) 7486904.

[14] C. Bonifácio, D. Ribeiro, R. Calçada, R. Delgado, Dynamic Behaviour of a Short Span Filler-Beam Railway Bridge under High Speed Traffic, in: Proc. 2nd Int. Conf. on Railway Technology: Research, Development and Maintenance, no. 79, 2014.

[15] E. Axelsson, A. Syk, M. Ülker-Kaustell, J.-M. Battini, Effect of Axle Load Spreading and Support Stiffness on the Dynamic Response of Short Span Railway Bridges, Structural Engineering International 24 (4) (2014) 457–465.

[16] L. Bornet, A. Andersson, J. Zwolski, J.-M. Battini, Influence of the ballasted track on the dynamic properties of a truss railway bridge, Structure and Infrastructure Engineering 11 (6) (2015) 796–803.

[17] L. R. Ticona Melo, J. Malveiro, D. Ribeiro, R. Calçada, T. Bittencourt, Dynamic analysis of the train-bridge system considering the non-linear behaviour of the track-deck interface, Engineering Structures 220 (2020) 110980.

[18] T. Rauert, H. Bigelow, B. Hoffmeister, M. Feldmann, On the prediction of the interaction effect caused by continuous ballast on filler beam railway bridges by experimentally supported numerical studies, Engineering Structures 32 (12) (2010) 3981 – 3988.

[19] A. Stollwitzer, J. Fink, T. Malik, Experimental analysis of damping mechanisms in ballasted track on single-track railway bridges, Engineering Structures (220) (2020) 110982.

[20] G. Nouri, Z. Ahmadi, Influence of Skew Angle on Continuous Composite Girder Bridge, Journal of Bridge Engineering 17 (2012) 617–623.

[21] AASHTO, LRFD bridge design specifications, 2010.

[22] Y. Deng, B.M. Phares, L. Greimann, G.L. Shryack, J.J. Hoffman, Behaviour of curved and skewed bridges with integral abutments, Journal of Constructional Steel Research (109) (2015) 115–136.

[23] A. Abdel-Mohti, G. Peckan, Seismic response of skewed RC box-girder bridges, Earthquake Engineering and Engineering Vibration 7 (4) (2008) 415–426.

[24] M. Mallick, P. Raychowdhury, Seismic analysis of highway skew bridges with nonlinear soil-pile interaction, Transportation geotechnics 3 (2015) 36–47.

[25] J.Y. Meng, E.M Lui, Seismic analysis and assessment of a skew highway bridge, Engineering Structures 22 (11) (2000) 1433–1452.

[26] B. Zakeri, J.E. Padgett, G.G. Amiri, Fragility Analysis of Skewed Single-Frame Concrete Box-Girder Bridges, Journal of Performance of Constructed Facilities 28 (3) (2014) 571–582.

[27] P. Ryjáček, M. Polák, T. Plachý, J. Kašpárek, The dynamic behaviour of the extremly skewed railway bridge "Oskar", Procedia Structural Integrity 5 (2017) 1051–1056.

[28] M. Jahangiri, J.A. Zakeri, Dynamic Analysis of Two-lane Skewed Bridge and High-speed Train System, Periodica Polytechnica Civil Engineering 63 (3) (2019) 695–708.

[29] M. Martínez-Rodrigo, E. Moliner, A. Romero, G. De Roeck, P. Galvín, Maximum resonance and cancellation phenomena in orthotropic plates traversed by moving loads: Application to railway bridges, International Journal of Mechanical Sciences 169 (2020) 105316.

[30] E. Moliner, A. Romero, P. Galvín, M.D. Martínez-Rodrigo, Effect of the end cross beams on the railway induced vibrations of short girder bridges, Engineering Structures 201 (2019) 109728.

[31] E. Reynders, System identification methods for (operational) modal analysis: Review and comparison, Archives of Computational Methods in Engineering 19 (1) (2012) 51–124.

[32] P. Galvín, A. Romero, E. Moliner, G. De Roeck, M. D. Martínez-Rodrigo, On the dynamic characterisation of railway bridges through experimental testing, Engineering Structures 226 (2021) 111261.

[33] ANSYS Mechanical, Finite Element Analysis (FEA) Software for Structural Engineering (17.1).
URL `https://www.ansys.com/products/structures/ansys-mechanical`

[34] P. Lou, A vehicle-track-bridge interaction element considering vehicle's pitching effect, Finite Elements in Analysis and Design 41 (4) (2005) 397–427.

[35] R. A. Clark, P. A. Dean, J. A. Elkins, S. G. Newton, An Investigation into the Dynamic Effects of Railway Vehicles Running on Corrugated Rails, Journal of Mechanical Engineering Science 24 (2) (1982) 65–76.

[36] A. Doménech, P. Museros, M. Martínez-Rodrigo, Influence of the vehicle model on the prediction of the maximum bending response of simply-supported bridges under high-speed railway traffic, Engineering Structures 72 (2014) 123 – 139. `doi:http://doi.org/10.1016/j.engstruct.2014.04.037`.

[37] Ministerio de Fomento, Gobierno de España, IF3 - Instrucción para el proyecto y construcción de obras ferroviarias, 2015.

[38] INTEMAC, Informe de resultados y conclusiones de las actividades de inspección técnica y prueba de carga realizadas en la estructura del puente P.K. 11+184, del tramo El Emperador-Ciudad Real sobre el río Jabalón.

[39] R. J. Allemang, The Modal Assurance Criterion Twenty Years of Use and Abuse, Journal of Sound and Vibration (37) (2003) 14–23.

[40] J. Haataja, Using Genetic Algorithms for Optimization: Technology Transfer in Action. In: John Wiley & sons Ltd, editor., Evolutionary Algorithms in Engineering and Computer Science (0-471-99902-4) (1999) 1–19.

[41] J. Malveiro, D. Ribeiro, C. Sousa, R. Calçada, Model updating of a dynamic model of a composite steel-concrete railway viaduct based on experimental tests, Engineering Structures 164 (2018) 40–52.

[42] J. Malveiro, D. Ribeiro, R. Calçada, R. Delgado, Updating and validation of the dynamic model of a railway viaduct with precast deck, Structure and Infrastructure Engineering 10 (11) (2014) 1484–1509.

[43] UNE-EN 13674-1:2006, Railway applications - track - rail - part 1: Vignole railway rails 46 kg/m and above, Spanish Norm CTN 25 - APLICACIONES FERROVIARIAS, Asociación Española de Normalización y Certificación, AENOR (2006).

[44] K. Nguyen, J. M. Goicolea, F. Galbadón, Comparison of dynamic effects of high-speed traffic load on ballasted track using a simplified two-dimensional and full three-dimensional model, Proceedings of the Institution of Mechanical Engineers, Part F: Journal of Rail and Rapid Transit 228 (2) (2014) 128–142.

[45] W. M. Zhai, K. Y. Wang, J. H. Lin, Modelling and experiment of railway ballast vibrations, Journal of Sound and Vibration 270 (4-5) (2004) 673–683.

[46] Ministerio de Fomento, Gobierno de España, IAPF 2010 - Instrucción de acciones a considerar en el proyecto de puentes

de ferrocarril, 2010.

[47] K. Liu, G. Lombaert, G. De Roeck, Dynamic Analysis of Multispan Viaducts with Weak Coupling between Adjacent Spans, Journal of Bridge Engineering 19 (1) (2014) 83–90.

[48] A. M. Moazam, N. Hasani, M. Yazdani, 3D simulation of railway bridges for estimating fundamental frequency using geometrical and mechanical properties, Advances in Computational Design 2 (4) (2017) 257–271.

[49] Ministerio de Fomento, Gobierno de España, lnstrucción de hormigón estructural, 2010.

[50] B. R. Cruz Cal, B. F. Guerra Valdés, E. A. Álvarez García, R. Alfonso Blanco, Evaluación de elastómero vulcanizado (Parte II) 72 (570) (2015) 133–137.

[51] E. Moliner, M. Martínez-Rodrigo, P. Galvín, J. Chordà-Monsonís, A. Romero, On the vertical coupling effect of ballasted tracks in multi-span simply-supported railway bridges under operating conditions, Structure and Infrastructure Engineering (2022) 1–23.

[52] J. Chordà-Monsonís, A. Romero, E. Moliner, P. Galvín, M. Martínez-Rodrigo, Ballast shear effects on the dynamic response of railway bridges, Engineering Structures 272 (2022) 114957. doi:https://doi.org/10.1016/j.engstruct.2022.114957.